The Planetary Science Journal, 5:231 (25pp), 2024 October https://doi.org/10.3847/PSJ/ad781e

Evaluating the Use of Unoccupied Aircraft Systems (UASs) for Planetary Exploration in Mars Analog Terrain

Brett B. Carr[1], Matthew Varnam[1], Nathan Hadland[1], Jahnavi Shah[2], Joana R. C. Voigt[1,3], Samantha Gwizd[3,4], Kathryn M. Stack[3], Fred Calef[3], Raymond Francis[3], Udit Basu[4], Baldur Björnsson[5], Colin X. Chen[6], Elisa Dong[2,7], Jeffrey E. Moersch[4], Michael Phillips[1], Joshua Springer[8], Catherine D. Neish[2], and Christopher W. Hamilton[1]
[1] Lunar and Planetary Laboratory, University of Arizona, 1629 East University Boulevard, Tucson, AZ 85721, USA; bbcarr@arizona.edu
[2] Department of Earth Sciences, University of Western Ontario, 1151 Richmond Street North, London, ON N6A 5B7, Canada
[3] Jet Propulsion Laboratory, California Institute of Technology, 4800 Oak Grove Drive, Pasadena, CA 91109, USA
[4] Department of Earth, Environmental, and Planetary Sciences, University of Tennessee, 1612 Cumberland Avenue, Strong Hall Room 602, Knoxville, TN 37996, USA
[5] Department of Engineering, Reykjavík University, Menntavegur 1, 101 Reykjavík, Iceland
[6] Honeybee Robotics, 2408 Lincoln Avenue, Altadena, CA 91001, USA
[7] Department of Earth and Space Sciences, York University, 4700 Keele Street, Toronto, ON M3J 1P3, Canada
[8] Department of Computer Science, Reykjavik University, Menntavegur 1, 101 Reykjavik, Iceland
Received 2024 May 23; revised 2024 August 30; accepted 2024 September 4; published 2024 October 17

Abstract

Planetary analog mission simulations are essential for testing science operations strategies and technologies. They also teach us how to use terrestrial analogs to inform studies of extraterrestrial environments. Unoccupied aircraft systems (UASs) have great potential for planetary surface exploration as demonstrated by the Mars 2020 Ingenuity helicopter and the in-development Dragonfly mission to Saturn's moon Titan. Although applications of UAS technology for planetary exploration remain largely unexplored, simulated missions in planetary analog terrains can inform operational best practices. As part of the Rover–Aerial Vehicle Exploration Network project, we simulated a 12 sol UAS mission on Mars in the Holuhraun region of Iceland. The UAS had airborne imaging capability, as well as imaging, sampling, and geochemical analysis capabilities while landed. The mission evaluated the use of these instruments and developed operational strategies for using UASs to explore a planetary surface. Oblique airborne images were essential for mission planning and were used to scout large areas to identify both potential landing sites and targets for focused investigations. The airborne and landed data collected by the UAS allowed for detailed observations and interpretations not possible with analog orbital data sets, resulting in an improved scientific return for the simulated UAS mission compared to a premission analysis of only the analog orbital data. As a planetary exploration vehicle, a UAS is most advantageous for exploring large areas (many square kilometers) and is particularly useful when the terrain may be impassable to ground-based traverses (e.g., by rovers or humans).

Unified Astronomy Thesaurus concepts: Volcanism (2174); Surface processes (2116); Earth (planet) (439); Mars (1007); Space vehicle instruments (1548)

1. Introduction

Unoccupied aircraft systems (UASs), also referred to as planetary aerial vehicles or surrogate aerial robots in the context of planetary exploration (e.g., L. A. Young et al. 2021), offer a novel and promising method of investigating planetary surfaces (e.g., M. R. James et al. 2020; G. Tmusic et al. 2020; M. Velez-Nicolas et al. 2021; C. G. Andresen & E. S. Schultz-Fellenz 2023). The Ingenuity technology demonstration (J. Balaram et al. 2021), associated with the Mars 2020 mission, demonstrated flight on an extraterrestrial body for the first time on 2021 April 19 and opened new frontiers for planetary surface exploration. Additionally, NASA's Dragonfly mission will use a ∼450 kg UAS to explore Saturn's largest moon, Titan (R. D. Lorenz et al. 2018; J. W. Barnes et al. 2021). UASs may also be part of the Mars Sample Return campaign (B. K. Muirhead et al. 2020; F. Mier-Hicks et al. 2023; National Academies of Sciences, Engineering, & Medicine 2023). As the technology continues to develop, UASs will become an increasingly important component of planetary exploration mission design and operation, which makes optimizing practices for their use in planetary environments essential.

Field-based testing of new mission architectures and science operations protocols can aid in the development of future Mars Science Helicopter (MSH) mission concepts (e.g., J. Bapst et al. 2021). Future missions could include either a stand-alone UAS or a multiagent network involving one or more UAS(s) operating in tandem with a lander or rover. However, determining how best to allocate resources is a complex task, which can be aided by field-based mission simulations (e.g., G. Pisanich et al. 2004; L. A. Young et al. 2004; G. R. Osinski et al. 2019; R. A. Yingst et al. 2020; S. Gwizd et al. 2024). Power limitations, data bandwidth, and instrument capabilities place constraints on vehicle operations and the activities that can be conducted to achieve mission objectives. Simulated missions in analog terrain can test trade-offs between these mission elements and develop operational strategies that can guide prioritization of science activities and plan building for future missions.

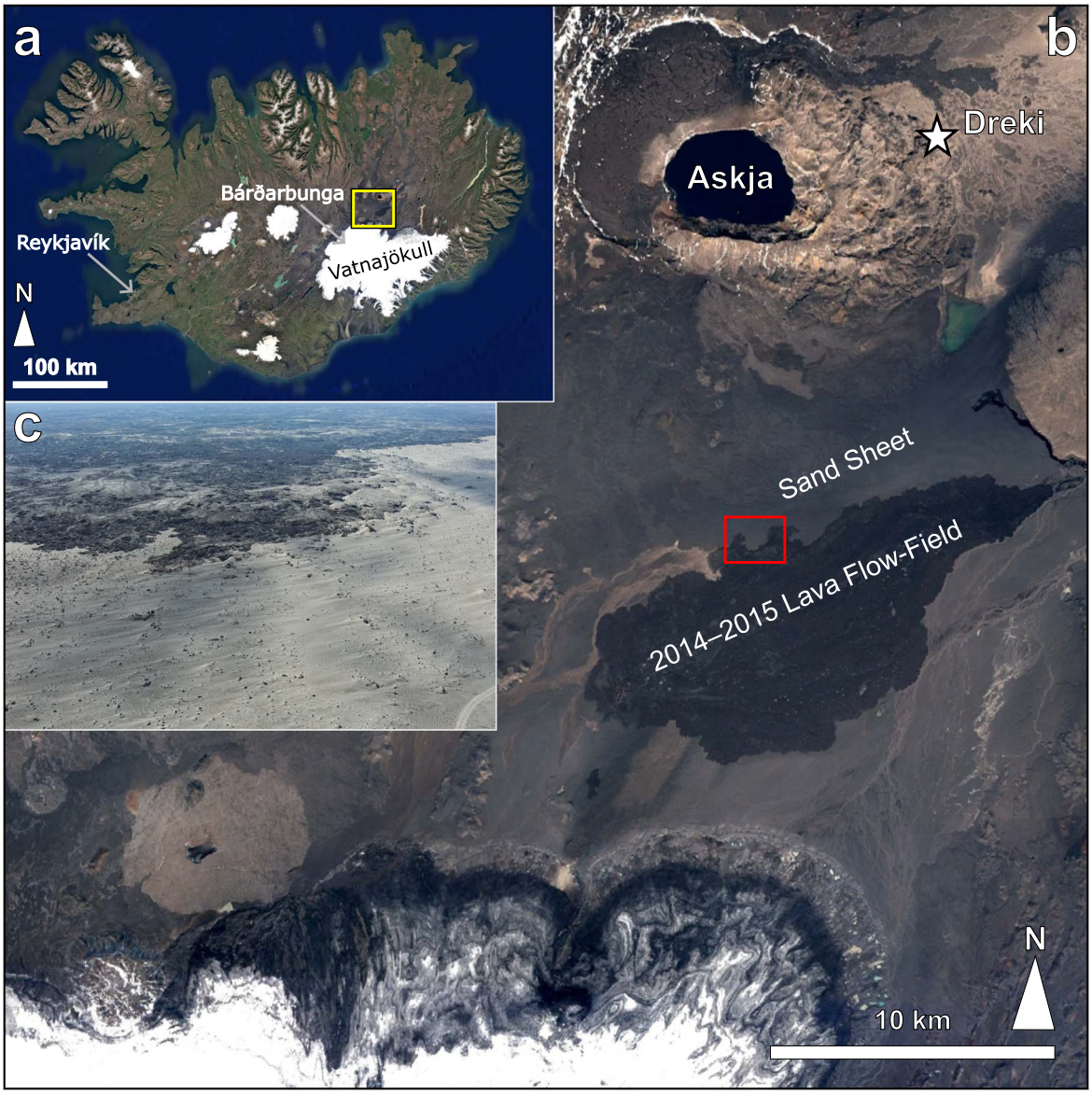

Figure 1. Location of Holuhraun. (a) The Holuhraun region and 2014–2015 lava flow field are located in the central highland of Iceland (yellow box). (b) The UAS mission was implemented along a stretch of the north-central flow-field margin (red box), while science operations were conducted at Dreki, near Askja volcano (star). (c) An airborne image taken from the northeast corner of the red box in (b) looking to the southwest shows the sand sheet in the foreground and 2014–2015 lava flow field in the background.

The Rover–Aerial Vehicle Exploration Network (RAVEN) addresses challenges that planetary UAS mission concepts will face through field-based simulations of UAS and rover mission architectures within a high-fidelity Mars analog terrain at Holuhraun, Iceland (Figure 1; S. Gwizd et al. 2024; J. R. C. Voigt et al. 2024). The primary goal of the RAVEN project was to develop and evaluate new technologies and science operations concepts for future Mars missions to determine the advantages and limitations of multiagent missions in comparison. RAVEN includes components related to technology and science operations. New technologies include (1) design, fabrication, and testing of new UAS-based samplers, including scoop and drill sampler systems, and (2) development and testing of UAS-enabled onboard image processing algorithms that use UAS data to improve rover localization. RAVEN also includes an operational component to explore the complexities of rover and UAS science operations within a Mars analog environment. During the 2022 field campaign in the Holuhraun region of Iceland, we developed baseline rover and UAS stand-alone mission simulations with which to compare future combined rover and UAS mission architectures.

Here, we describe the development, results, and lessons learned of the 2022 stand-alone UAS mission. The goals of this simulated mission were to (1) develop operational strategies for using UASs to explore a planetary surface, (2) evaluate a suite of instruments for use on a UAS, and (3) assess how operational strategies and instruments can be used to maximize the scientific return of a UAS mission. S. Gwizd et al. (2024) describe the stand-alone rover simulated mission conducted concurrently with the UAS mission simulation.

The Holuhraun region of Iceland (Figure 1) has been shaped by volcanic, glacial, hydrological, and eolian processes. The 2014–2015 Holuhraun eruption extruded lava with a dense rock equivalent volume of 1.2 km^3 that covered an area of 84 km^2 (E. Bonny et al. 2018). This was the largest effusive

eruption in Iceland since the 1783–1784 Laki eruption (T. Thordarson & G. Larsen 2007). Magma feeding the 2014–2015 Holuhraun eruption was sourced from beneath the Bárðarbunga central volcano but traveled 48 km laterally to the northeast before erupting to emplace lava onto a barren, flat-lying proglacial landscape (M. T. Gudmundsson et al. 2016). Lava partially inundated the Dyngjussandur flood plain, older basaltic lava flows, and tributaries of the Jökulsá á Fjöllum river north of the Vatnajökull ice cap (M. E. Hartley et al. 2016; L. E. Bonnefoy et al. 2019; J. R. C. Voigt et al. 2021a). The large lava volume, barren terrain without vegetation, and similarities of lava surfaces to other planetary volcanic terrains make the 2014–2015 Holuhraun eruption a valuable analog site and provide insights into the dynamics and evolution of large effusive eruptions on other planetary bodies (J. R. C. Voigt et al. 2022, 2023). Specifically, the Holuhraun region is analogous to young volcanic terrains on Mars, such as Elysium Planitia (Voigt et al., this issue). Elysium Planitia is the youngest volcanic terrain on the planet and shares many similarities to Holuhraun, including but not limited to the extensional tectonic setting combined with a potential mantle plume (S. C. Stahler et al. 2022; A. Broquet & J. C. Andrews--Hanna 2023), many fissure-fed eruptions (J. R. C. Voigt et al. 2023), and lava morphologies. Considering the roughness of different lava morphologies (J. R. C. Voigt et al. 2021b; G. D. Tolometti et al. 2022) and the difficulty of traversing over these surfaces on the ground (e.g., by rovers or humans), science operations and technology testing involving UASs conducted at Holuhraun has direct relevance to potential sites for future Mars surface exploration.

2. Mission Development

2.1. UAS Design

We developed UAS operations based on conceptual designs for an MSH (W. Johnson et al. 2020; J. Bapst et al. 2021). The MSH would build on the Ingenuity technology demonstration (J. Balaram et al. 2021) by adding scientific instrumentation. As a result, the proposed MSH would carry considerably more payload than Ingenuity, with a potential flight time of approximately 6 minutes (before needing to recharge the battery) when carrying a 5 kg scientific payload (W. Johnson et al. 2020). To fly this mass, the future MSH would need to be much larger, approximately 31 kg unburdened, compared to Ingenuity's 1.8 kg. To simulate the capabilities of an MSH-like UAS, our simulation used instruments on board two commercial UASs along with handheld instruments for landed observations.

We selected scientific instrumentation for the UAS that would allow the UAS Science Operations Team to (1) address science questions motivated by the RAVEN Science Traceability Matrix (STM; Table 1 and Section 2.3) and (2) assess the benefits and limitations of each instrument for use on a future MSH. The instruments selected for the UAS included (1) a fixed focal length airborne imaging camera, (2) a fixed focal length microimaging camera for landed images of the ground, (3) a laser-induced breakdown spectrometer (LIBS) to measure the elemental composition of the surface, (4) a point spectrometer in the visible light to near-infrared (VISIR) wavelengths to determine mineralogy, and (5) sampling capabilities, which included a scoop and drill and the ability to transport one collected sample at a time. We assume that an airborne imaging camera on board a future MSH would be mounted on a single-axis gimbal underneath the front of the UAS body, allowing for look angles ranging from 0° (horizontal) to 90° (vertical, or nadir). A free axis for rotation (yaw) is considered unnecessary for near-term MSH designs because the pointing direction of the camera can be controlled by pivoting the orientation of the UAS. A third axis (roll) of rotation can help to orient the camera to the horizon but is not strictly necessary given other forms of camera stabilization (e.g., R. Ljubicic et al. 2021). The sampling apparatus for a future MSH would be mounted underneath the center of the UAS body and collect a sample from the surface upon which the UAS landed. The microimager, LIBS, and VISIR spectrometer would also be mounted underneath the UAS and aimed at the same location below the UAS to allow colocation of data collection and sampling.

Energy is a limiting factor for UAS operations on Mars. The MSH proposal includes a battery with 1.2–1.4 MJ (333.33–388.89 Wh) of usable energy (70% of total stored energy to allow for reserves and extend battery life; W. Johnson et al. 2020). We used the lower bound of 333.33 Wh sol^{-1} as the power usage cap. A small amount of this energy is needed to keep the UAS warm throughout the sol. We apply the formula of W. Johnson et al. (2020), which scales sleep energy relative to Ingenuity by the cube root of the UAS mass. For flight, we set the power draw to use the available battery energy in ∼6 minutes to align with the hover-time estimates of W. Johnson et al. (2020) for a 5 kg payload. We determined the power usage for each instrument using estimates from analog instruments (e.g., Mastcam-Z and ChemCam) and created an activity dictionary (Table 2) and power budget calculators to plan each sol within the imposed limit.

We imposed two restrictions on data transmission during the mission. The first was a hard cap of 140 MB day^{-1}, and the second was a soft cap by applying an energy cost to transmission. The 140 MB day^{-1} hard cap derives from data return rates from Mars 2020 ultra-high-frequency (UHF) communications through orbiting satellites such as the Mars Reconnaissance Orbiter,[9] assuming four to five satellite overpasses on any given sol. Unlike Ingenuity, which uses a lightweight, lower-power communications system reliant on Perseverance as a relay for data transmission (J. Balaram et al. 2021), our UAS must be capable of operating independently. Like Perseverance itself, the UAS requires a higher-power transmission system capable of communicating with an orbiting satellite. As a compromise for using a lower mass than Perseverance to meet the requirements of a 0.1 kg transmission system from W. Johnson et al. (2020), we lowered our bit rate to 420 kbps (compared to a 3 kg transceiver capable of 2 Mbps for Perseverance[10]) while keeping the same power usage of 65 W.

2.2. Site Selection and Mission Parameters

Following an initial examination of potential mission start locations and exploration areas, a start location was chosen near the northern margin of the Holuhraun lava flow field (Figure 2) that balanced mission priorities with logistical constraints, trafficability constraints, and hazard assessments for the rover and UAS (see below). A separate hazard analysis

[9] https://Mars.nasa.gov/msl/mission/communications/
[10] https://Mars.nasa.gov/mars2020/spacecraft/rover/communications/

Table 1
High-level Goals from the RAVEN STM

Science Goals	Science Objectives	Achieved
MEPAG science goal 1: determine if Mars ever supported, or still supports, life	(1) Search for evidence of hydrologic activity; if present, acquire data to characterize hydrologic features and constrain habitability	Yes: identified potential glacial outburst flood deposits and that the younger lava flow field may have been emplaced over a fluvial region
Decadal survey question 10: dynamic habitability		Yes: used data collected to assess habitability
Decadal survey question 11: search for life elsewhere	(2) Collect geochemical data and samples of rocks and sediments (three samples total) that can be used to constrain potential habitability	Yes: a sediment sample was taken at a location where the VISIR spectrometer detected hydration
		Yes: detected hydration using VISIR spectrometer at a white discoloration on younger lava surface
MEPAG science goal 2: understand the processes and history of climate on Mars	(1) Search for eolian bedforms; if present, acquire data to characterize any bedforms observed to constrain the rates, fluxes, and atmospheric conditions associated with active eolian transport	Yes: identified wind ripples and other eolian bedforms; determined a northeastern transport direction
Decadal survey question 10: dynamic habitability		Yes: images and survey products provide data that can be used to constrain transport rates and fluxes
MEPAG science goal 3: understand the origin and evolution of Mars as a geologic system	(1) Search for sedimentary deposits; if present, collect geochemical data of the material that can be used to constrain sediment composition and provenance	Yes: measured sediment with LIBS and VISIR spectrometer and determined a basaltic composition for all material
Decadal survey question 5: solid-body interiors and surfaces		Yes: collected a sample of sediment
		Yes: geochemical data and samples collected can be used to interpret sediment provenance
	(2) Search for lava units; if present, collect geochemical data of lava that can be used to constrain their composition and inform volcanic processes on the surface, within the crust, and in the interior	Yes: measured the younger lava with the LIBS and VISIR spectrometer and determined a basaltic composition
		Yes: collected two samples of the younger lava
		Yes: geochemical data and samples collected can be used to interpret volcanic and magmatic processes
	(3) Search for volcanic features on the surface; if present, acquire data to characterize observed features and constrain the eruptive history of the area	Yes: identified two separate eruptive events, the older lava flow and younger lava flow field
		Yes: the period between eruptions was long enough for sediment to be deposited by eolian processes on the older lava flow and mostly bury it
	(4) Search for volcanic features related to lava flow emplacement; if present, acquire data to characterize observed features and constrain emplacement conditions	Yes: younger lava flow field in the mission area identified as "spiny" morphology, a transitional lava type between pāhoehoe and ʻaʻā
		Yes: an eruption sequence with multiple flow lobes was determined for the younger lava flow field; eruption rate and duration were estimated for the emplacement of the younger lava flow field

Note. The science goals (first column) and objectives (second column) from the RAVEN STM guided planning for the UAS mission. The third column is an assessment of whether the goal was achieved during the mission (Section 5.5).

(Section 2.3.1) and mapping of regions of interest for science investigations (Section 2.3.2) were performed for the stand-alone UAS mission simulation, separate from the rover mission simulation.

The Science Operations Teams for the concurrent rover and UAS stand-alone simulated missions worked together to create shared science goals, operational goals, and practical considerations that would be followed by both vehicles to allow direct comparison of mission metrics (S. Gwizd et al. 2024). Shared operational constraints included that the missions should begin at the same location, each last at least 10 implemented sols, and include collection of at least three samples to be cached together in one location. The mission start location (Figure 2) was restricted to places that were accessible via road by the truck transporting the rover and close enough to the 2014–2015 Holuhraun lava flow field that the rover could reach the flow margin during a 10 sol mission (∼500 m; S. Gwizd et al. 2024). Once the mission simulations began, the rover and UAS Science Operations Teams operated in parallel but independently.

The science objectives for the missions were guided by the RAVEN project STM. Table 1 summarizes these objectives, which are linked to priorities outlined in the "Planetary Science and Astrobiology Decadal Survey 2023–2032" (National Academies of Sciences, Engineering, & Medicine 2023) and the Mars Exploration Program Analysis Group (MEPAG) Science Goals document (MEPAG 2020). The objective at the end of the mission was for the Science Operations Teams to use the data collected to develop an interpretation of the mission terrain, including a description of the chemical composition of

Table 2
UAS Activity Dictionary

UAS Activity	Description	Power (W)	Processed Data Collected (MB s^{-1})
Operation			
Sleep	Power use for keeping warm	1.6	N/A
Spin up	Requires 10 s rotor spin-up before takeoff	1584.5	0.07
Takeoff	Increase altitude at 1 m s^{-1}	3234.0	0.07
Ascend	Increase altitude at 5 m s^{-1}	3493.6	0.07
Hover	Hover in place	3169.1	0.07
Flight (fast)	Level flight at 15 m s^{-1}	2545.1	0.07
Flight (slow)	Level flight at 5 m s^{-1}	3169.1	0.07
Descend	Decrease altitude at 5 m s^{-1}	3169.1	0.07
Landing	Decrease altitude at 1 m s^{-1} and power off	3169.1	0.07
In-flight Instruments			
Camera (standby)	Camera standby 60 s for warm-up	7.5	<0.01
Camera (high quality)	Requires 5 s camera use	12.0	1.49
Camera (low quality)	Requires 5 s camera use	12.0	0.45
Mapping survey	Flight and camera operation	3181.1	<0.01
Laser altimeter	Continuous laser altimeter for navigation during flight	1.5	<0.01
Contact Science Instruments			
LIBS (power on)	Requires 600 s, power on LIBS	24.0	<0.01
LIBS (measurement)	Requires 144 s, fire LIBS for one point	50.0	0.02
LIBS (power off)	Requires 240 s, power off LIBS	15.0	<0.01
VISIR measurement	Hyperspectral measurement requires 144 s	50.0	0.02
Microimage	Requires 5 s camera use	12.0	1.49
Drill sample	240 Wh/6 cm, requires 1 hr duration	280.0	<0.01
Data			
Data processing (full)	Process mapping survey images to create orthomosaic and DEM at resolution specified	5.0	0.10
Data processing (data light)	Process mapping survey images for DEM at 20 cm $pixel^{-1}$	5.0	0.01
Transmit data	Use Electra-Lite UHF to transmit at 187.5 MB hr^{-1}	65.0	N/A

Note. Each activity that the UAS could perform (first column) had a known power consumption rate (third column) and data creation rate (fourth column). For each sol, a calculator was used to input the duration of each planned activity and calculate the power usage and data volume for the sol. The plan was modified until the power and data used were within the caps imposed on the UAS.

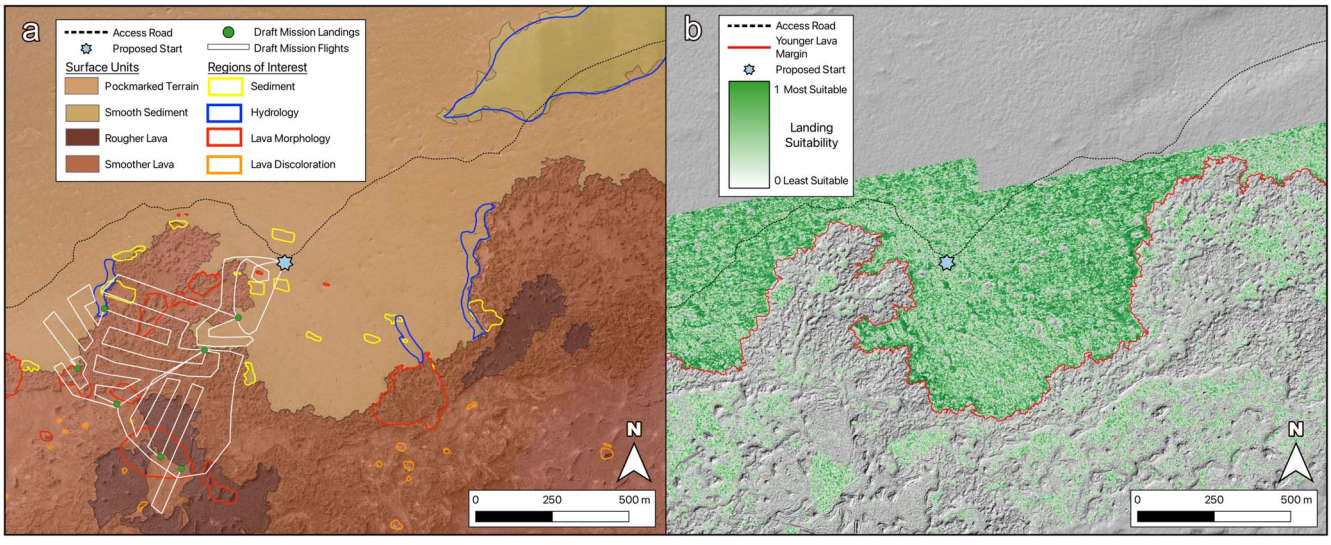

Figure 2. Premission strategic planning. The Science Operations Teams identified four main surface units in the mission area (a) and a starting location for the mission (light blue marker). The UAS Science Operations Team identified regions of interest for each surface unit (colored outlines, (a)) and developed a draft mission plan (white flight lines and green landing markers, (a)) in order to achieve the mission objectives in the prescribed timeline. The UAS landing suitability map (b) was created by combining three different ground surface parameters using the DEM. Darker green represents more suitable landing locations, lighter green represents less suitable locations, and areas with no data are unsuitable for landing. The (a) orthomosaic and (b) DEM hillshade base maps are from a 2015 survey by Loftmyndir ehf. and a 2018 UAS survey (S. P. Scheidt & C. W. Hamilton 2021). The black dashed line is the road used to access the site. Surface unit polygons are modified from J. R. C. Voigt et al. (2021a). The landing suitability analysis was conducted using the more detailed 2018 UAS survey, which only covered the lava flow margin in the southern half of the map extent.

the geologic units present, a geologic history of the region, and an assessment of the potential habitability of the area.

2.3. Strategic Planning

The rover and UAS Science Operations Teams conducted a premission analysis of the mission area to choose a mission start location, science targets, and an initial mission plan. For these tasks, the Science Operations Teams were provided orthomosaics at 0.25 m pixel^{-1} and digital elevation models (DEMs) at 1.0 m pixel^{-1}. Data sources included UAS and airborne survey products (J. R. C. Voigt et al. 2021a; S. P. Scheidt & C. W. Hamilton 2021; Loftmyndir ehf.) that were reprocessed such that the resolution matched that of the DEMs and orthomosaics produced from stereo images captured by the High Resolution Imaging Science Experiment (HiRISE) camera on the Mars Reconnaissance Orbiter (A. S. McEwen et al. 2007; S. S. Sutton et al. 2022). The Science Operations Teams were also provided with two 1:800-scale geomorphological maps illustrating (1) different surface facies of the 2014–2015 Holuhraun lava flow field (J. R. C. Voigt et al. 2021a) and (2) context outside of the Holuhraun lava flow field. Both mapping products are based on differences in color (i.e., albedo at red, blue, and green wavelengths), surface texture, and morphologies as they appear in a 0.2 m pixel^{-1} UltraCam-Xp base map (acquired on 2015 September 6; J. R. C. Voigt et al. 2021a).

Using these data sets, the Science Operations Teams determined that the region was dominated by volcanic landforms, including lava that covers the southern half of the exploration area (Figure 2). Sand mantles much of the area. The Science Operations Teams created a premission surface morphology map focusing on descriptive terms and avoiding interpretations of the different units (Figure 2(a)). This map identified two dominant lava morphologies (rougher and smoother), two sediment morphologies (pockmarked terrain and smooth sediment), and areas of interest (blue outlines; Figure 2(a)) for the hydrologic objectives in the STM (Table 1). Further analysis of the provided data sets and discussion among the Science Operations Teams determined that the pockmarked terrain was likely due to the sediment covering older lava (in contrast to the younger lava that was clearly visible), and this surface was generally referred to as the "older lava" during and after the mission. These initial observations and the STM (Table 1) led the UAS Science Operations Team to attempt to answer four key questions during the mission: (1) what is the geologic history of the region? (2) What was the emplacement sequence for the younger lava? (3) How active is eolian transport and what is the source of the sediment? and (4) Is there evidence of past and/or present hydrologic activity?

2.3.1. UAS Landing Site Requirements

Any landing site for the UAS chosen by the UAS Science Operations Team during the mission had to be accessible to the UAS Field Implementation Team on foot. The presence of the UAS Field Implementation Team was required so that they could maintain a visual line of sight and safely monitor the landing of the UAS and use handheld instruments to conduct landed science measurements (i.e., LIBS, VISIR, microimage) and sampling activities (Section 3.4). This restriction meant that many parts of the 2014–2015 lava flow field were designated as "no landing" zones due to their inaccessibility to the UAS Field Implementation Team, even though they were technically within the flight range of the UAS. To minimize risks for team members and protect equipment, the UAS Science Operations Team designed their flight plans to remain within ~1500 m of the starting location on the sand sheet (roughly the extent of the map in Figure 2). Restricting the mission area in this way would not impact the mission goals related to developing operations strategies and evaluating instrumentation. Although this would prevent the UAS from targeting regions of the younger lava with scientific interest to the UAS Science Operations Team (e.g., the eruption's source vents and central lava pathway), the terrain within the designated mission area was suitable for achieving all science objectives (Table 1) and addressing the key questions concerning the geology of the region.

The UAS Science Operations Team used the 1.0 m resolution DEM to create a hazard map of the mission area to inform landing suitability. The hazard map was a combination of three separate parameters calculated from the DEM using tools built into the Quantum GIS (QGIS) software[11]: (1) slope, (2) roughness, and (3) terrain ruggedness index (TRI; S. J. Riley et al. 1999). Slope in QGIS is calculated using a weighted average of the gradients between a central pixel and its eight neighboring pixels (B. K. P. Horn 1981). The roughness calculation returns the difference between the maximum and minimum elevations in a 3 by 3 pixel neighborhood. The TRI calculation returns the mean of the absolute values of the elevation differences between a central pixel and its neighbors (M. F. J. Wilson et al. 2007). All three parameters are useful for assessing landing suitability, as slope measures the trend of elevation changes while roughness is sensitive to a single outlier pixel elevation and TRI is sensitive to elevation variations over the entire pixel neighborhood.

In the absence of specifications regarding landing hazards for an MSH (W. Johnson et al. 2020; J. Bapst et al. 2021), maximum allowed values for each of the parameters were defined based on the specifications for the UAS being used in the field (Section 3.3). These values were 5° for slope, 0.3 m for roughness, and 0.1 m for TRI. Any pixel with a larger value for any parameter was defined as unsuitable for landing. The slope, roughness, and TRI values of the remaining pixels (where slope $\leqslant$5°, roughness $\leqslant$0.3 m, and TRI $\leqslant$0.1 m) were then normalized such that a value of 1 corresponded to a parameter value of 0 (i.e., a flat surface for each parameter) and the most suitable landing surface. The landing hazard map was calculated by averaging the normalized values for each parameter and had values ranging from near 0 (unfavorable landing location) to near 1 (most favorable landing location) and included "no data" pixel values where landing was not possible (Figure 2(b)).

Lastly, a 5 m uncertainty radius in the UAS landing was manually induced by the UAS Field Implementation Team. While we assume a future MSH would have a robust autonomous landing capability (e.g., R. Brockers et al. 2021), we did not have the ability to simulate a similar system during this mission. The manual landings avoided potential damage to the UAS from hazards that were unseen in the premission mapping phase (Figure 2). The manual adjustments also introduced some positioning error into the executed UAS flight plans to more realistically simulate flights that would

[11] www.qgis.org

involve automated hazard detection and avoidance during landing. Automated adjustments to prespecified landing locations would be expected during an actual MSH mission through a combination of computer vision and automated hazard detection and avoidance systems that would build on the Jet Propulsion Laboratory's previously demonstrated guidance, navigation and control (A. E. Johnson et al. 2023), and autonomous science capabilities (R. Francis et al. 2017). The landing precision of the UAS (∼5 m) was thus larger than the 1.0 m resolution of the hazard map, so during the mission, the UAS Science Operations Team selected as landing locations large groupings of favorable pixels (darker green areas; Figure 2(b)).

2.3.2. Identification of Regions of Interest

After identifying the main surface units (Figure 2(a)), the UAS Science Operations Team selected and prioritized specific regions of interest in the mission area (colored outlines; Figure 2(a)) that appeared most likely to help develop an understanding of the region's geology and address the mission goals. Locations identified included sites representing the typical appearance of mapped surface units, contacts between units, and features that could not be interpreted at the resolution of the orthomosaic and DEM provided to the Science Operations Teams. Four potential sampling targets were also selected: (1) older lava, (2) younger lava, (3) sediment, and (4) a sample most likely to show evidence of hydrologic processes. It was possible that one sample could serve multiple purposes, but the final decision on sampling priority was deferred to the mission execution.

Locations to target during the stand-alone UAS mission were prioritized by (1) relevance to science objectives, (2) accessibility and proximity to the mission start location and each other, (3) appearance as an ideal example of a mapped surface unit, and/or (4) potential as a target for landed science activities. The ability to efficiently visit locations most helpful toward accomplishing the science and sampling goals would drive mission planning decisions. During the mission, regions of interest given lower priority in premission planning were used as opportunistic targets when observations could be made without diverting the resources needed for the UAS to visit a higher-priority target.

2.3.3. Operations Strategies

Based on the design and instrument payload of the UAS mission (Section 2.1), the UAS Science Operations Team created a list of data collection activities that could be used during the mission (Table 2). The airborne imaging camera would have modes for (1) oblique airborne photographs, (2) ascent or descent photographs at nadir (90° look angle), (3) photogrammetric mapping surveys (look angle of 85°, as slightly oblique angles improve mapping compared to nadir images; M. R. James & S. Robson 2014), and (4) landed imaging looking horizontal (0° look angle). To save on data transmission volume, images from mapping surveys were not downlinked. Instead, only processed DEMs and orthomosaics were returned at a resolution designated by the UAS Science Operations Team. This procedure simulates onboard photogrammetric processing, but during a real mission, individual images could be returned more gradually while the MSH is stationary between flights over a period of several sols. The UAS Science Operations Team generally planned to do microimage, LIBS, and VISIR measurements at each landing location regardless of sample acquisition, as these activities used relatively low amounts of power and data (Table 2). Sampling would require an entire day's power budget and would be preceded and followed by microimaging, LIBS, and VISIR observations to look for differences between the surface and near-subsurface.

The UAS Science Operations Team developed hypothetical 10 sol mission plans to test how the UAS could be used to address the goals of the mission. Different strategies were created to evaluate how best to (1) collect samples efficiently given the constraints that the UAS could carry only one sample at a time and all samples had to be cached in one location; (2) develop the breadth of the science target coverage given limits on the range of the UAS imposed by the power budget, sample cache, and UAS Field Implementation Team access to landing sites; and (3) balance survey flights and direct flights to high-priority targets. A consensus was reached where, based on the initially proposed mission start location (Figure 2), the first few sols of the simulated mission would include relatively short flights to conduct reconnaissance of the area and validate landing suitability assessments while focusing on visiting sand sheet and older lava targets. The second half of the mission would focus on assessing the younger lava. The mission strategy favored by the UAS Science Operations Team prior to the start of the simulation was to land at the highest-priority sites and use the photogrammetric survey capability of the UAS while flying to generate high-resolution maps of the area between subsequent landing locations. Ideally, landing sites would be spaced such that a contiguous map could be created following the mission. The result was a mission plan covering a relatively small area with a dense network of flight lines to return a high level of connected detail about the targeted region (Figure 2(a)).

3. Mission Implementation

3.1. Personnel

The UAS Science Operations Team oversaw all planning for the UAS mission and consisted of four members with roles of Lead, UAS Planner, Science Planner, and Documentarian. The Lead conducted planning meetings, made final decisions on UAS plans for each sol, ensured that the mission guidelines were followed, and worked with the UAS Field Implementation Lead to discuss execution of the daily plan and data downlink. The UAS Planner ensured that activities for the UAS in each sol fit within the power and data budgets (Table 2). The Science Planner worked with the UAS planner to translate UAS goals for a sol plan into specific activities and kept track of the STM to ensure that objectives were being met. The Documentarian kept records of all UAS Science Operations Team activities.

The UAS Field Implementation Team was charged with implementing the mission plan created by the UAS Science Operations Team and consisted of two Co-Leads, operators for the LIBS, VISIR spectrometer, and sampling instruments, and a Documentarian. The Co-Leads conducted the plan translation with the Science Operations Team Lead, operation of the UAS for the planned sol, and data downlink.

3.2. Plan Creation and Translation

The UAS Science Operations Team followed a scripted structure for planning each sol's operations based on the format used by the Mars Science Laboratory and Mars 2020 missions (S. M. Milkovich et al. 2022; A. R. Vasavada 2022). Planning began with an assessment of downlinked data from the previous sol and mission progress to date. The bulk of the planning meeting consisted of identifying science targets for the next sol and building a flight and science activity plan that fit within the daily power and data budgets. Plan building typically required multiple iterations as activities were added, modified, or removed until the plan satisfied both the resource constraints and the objectives defined by the team for that sol. Planning concluded with a forward-looking discussion focusing on "$N+1$" and "$N+n$" concepts for the subsequent sols (where "N" represents the current planning sol and "n" represents any number of sols in the future). The planning meeting was restricted to a duration of 2–3 hr to meet logistical constraints for the implementation of the plan at the field site each day.

Plan translation, the communication of the sol plan created by the UAS Science Operations Team to the UAS Field Implementation Team, occurred following the science planning meeting via a discussion and exchange of digital files between the team leads. The UAS flight plan was created using the universal Ground Control Software (UgCS)™, which allowed the UAS Science Operations Team to automate the precise locations and orientations of UAS takeoff and landing, imaging, and mapping surveys. The flight plan file was copied onto the UAS controller for activation in the field. Other instructions and a summary of data requested to be downlinked were communicated to the implementation leads via a Plan Translation Form. Following the plan translation meeting, no further communication between the operations and implementation teams was permitted.

3.3. Instrumentation and Software

A DJI Matrice 300 RTK™ UAS with a DJI Zenmuse P1™ 35 mm fixed focal length camera was used to implement the flight plan created by the Science Operations Team and capture images. An Apple iPhone 13 Pro™ was used for the microimager. Images from the P1 camera were downsized from ∼20 to ∼8 MB each using Apple Photos™ prior to downlink. Images from mapping surveys were processed using Agisoft Metashape Pro™ v1.8 to create orthomosaics and DEMs. Survey data products were exported at resolutions that were determined by the UAS Science Operations Team to fit within the data budget for downlink. The geotagged image locations provided spatial reference for the maps. Geotagging was enabled using a DJI Differential Real-Time Kinematic D-RTK 2 Mobile Station™ that was paired to the Matrice 300 UAS. Global navigation satellite system (GNSS) positioning is unrealistic for Mars applications, but it was assumed that a future MSH would have localization capabilities that would enable geotagging of UAS data relative to landmarks in geoencoded HiRISE images.

Two separate DJI Matrice 600™ UASs were modified for sampling, one equipped with a drill (for hard rock) and another with a variety of scoop attachments (for sediment). Due to the limitations of the UAS drill prototype and the risk of damaging the drill bit during basalt sampling operations, a hand drill was used instead when a lava sample was requested. Storage, transport, and caching of the samples by UAS were not simulated. Instead, after collection by scoop or drill, sample material was placed in labeled bags by the UAS Field Implementation Team.

The LIBS was a SciAps Z300™ handheld LIBS analyzer with a wavelength range of 200–900 nm. Five separate spectra were collected for each LIBS target designated by the UAS Science Operations Team. Each spectrum resulted in measurements of elemental abundance that were then converted to normalized oxide abundance and downlinked to the UAS Science Operations Team.

The VISIR point spectrometer was a Spectral Evolution OreXpress™ field spectrometer with a wavelength range of 350–2500 nm and spectral sampling of 2.8 nm channel^{-1} between 350 and 1000 nm and 6–8 nm at >1000 nm. VISIR data were collected with 1 s integration time, averaging 10 scans, and corrected to reflectance with internal dark current subtraction and division by a Spectralon white reference collected just before sample collection. Further processing to generate spectral plots and parameters to give to the UAS Science Operations Team were done in python using the HyPyRameter package (Phillips et al. 2024).

3.4. Field Implementation

The UAS Field Implementation Team Co-Leads initiated the UgCS™ flight plan created by the UAS Science Operations Team, and the Matrice 300 RTK™ UAS conducted the flight plan automatically. Matrice 300 RTK™ landings were conducted manually within a 5 m radius of the landing location that was defined by the UAS Science Operations Team. Flights were only conducted when environmental conditions were optimal for operation of the UAS and the presence of the Field Implementation Team at the site (e.g., winds and temperatures within the specifications of the Matrice 300 RTK™ and no active precipitation). Given the short duration of the flights (<6 minutes), an acceptable flight window occurred on most days, except for when inclement weather forced the complete cancellation of all field implementation activities. The LIBS, VISIR spectrometer, and microimager were operated by UAS Field Implementation Team members who would walk to the landing site following flight.

4. Results

4.1. UAS Mission Narrative

The UAS mission began in a large low-hazard area ∼200 m northwest of the margin of the younger lava (Figure 3). This site was ∼600 m east of the mission start location that was selected by the Science Operations Teams prior to deployment (Figures 2 and 3). The decision to change the mission start location was made because the truck delivering the rover to the field site could not transit the final few hundred meters to the chosen start location, and mission parameters dictated that the UAS and rover stand-alone missions begin at the same site. This new location was still within the exploration area that had been initially characterized by the rover and UAS teams.

The original plan for sol 101, the first day of simulated mission operations, had been to focus on the older lava and sand sheet (Figure 2(a)). However, due to the deviation from the proposed starting location, a new area of scientific interest was now within range of a single UAS flight. This was a

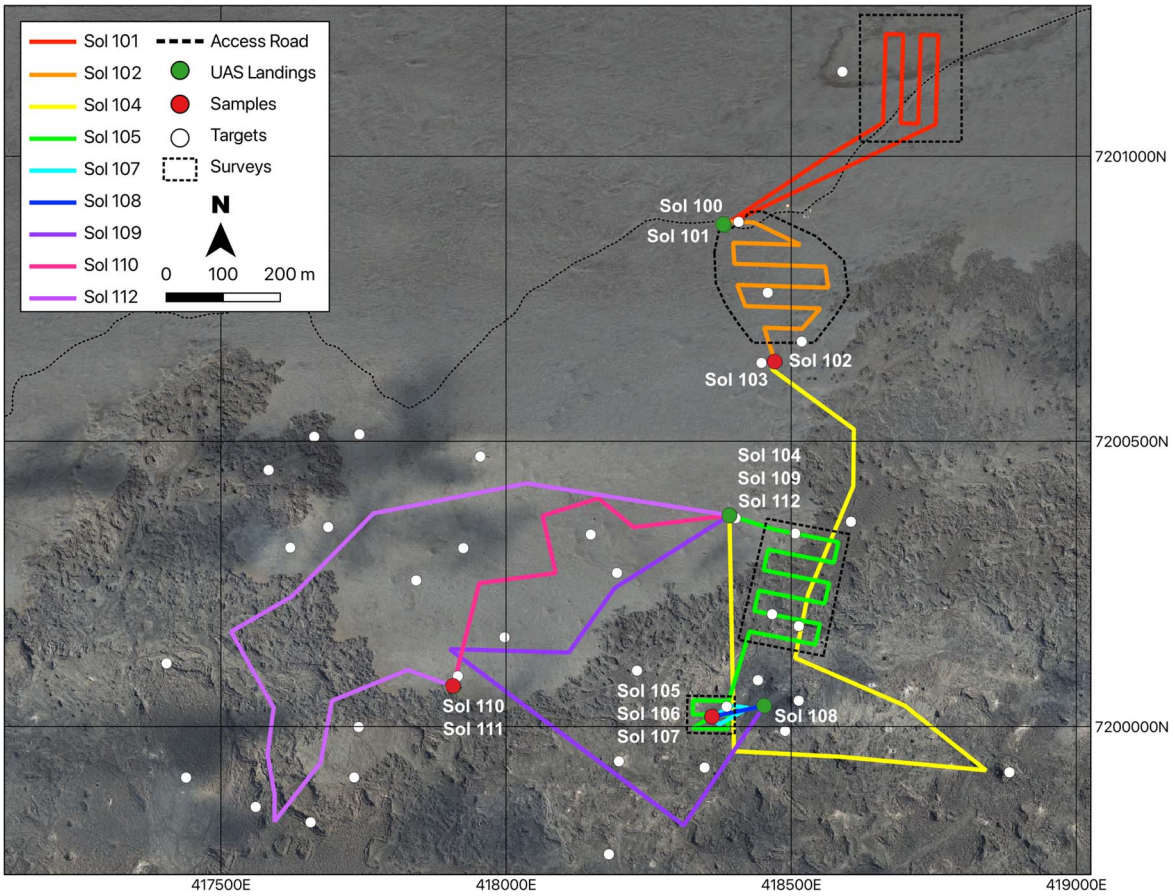

Figure 3. UAS mission. The UAS mission consisted of nine flights (colored solid lines) and six unique landing locations (green circles). Three samples were collected at the sol 102, sol 105, and sol 110 landing locations (red circles). White circles are targets specifically identified in planning for oblique airborne imaging. Mapping surveys were conducted on sols 101, 102, and 105 (dashed outlines). The sample cache was located at the shared landing site of the sol 104, 109, and 112 flights. The sol labels show the location of the UAS at the end of each mission sol. The base map is from a UAS survey of the field site conducted concurrently with (but not as a part of) mission implementation. The coordinate grid has a 500 m interval in WGS 84 UTM Zone 28N.

depression filled with sediment and boulders to the northeast of the mission start site classified in premission mapping as the "smooth sediment" surface (Figures 2(a), 3, and 4(a)). Despite being of high scientific interest during the premission analysis, this location had not been prioritized in planning because it was too far away from the proposed mission start location (Figure 2). The actual mission start location (Figure 3) provided quick access to this area without impacting the UAS Science Operations Team's ability to address other mission goals. The sediment in the depression lacked the outcroppings of the older lava in the pockmarked terrain unit (Figure 2(a)), suggesting that either the older lava was not present as a substrate or the sediment fill was thicker in this area. The UAS Science Operations Team took advantage of the unexpected proximity of this terrain and planned a mapping survey of the area for sol 101. Additionally on sol 101, the UAS captured oblique airborne photos looking to the southeast toward the younger lava. The UAS Science Operations Team used these images to scout for landing sites for future sols and correlate the landing suitability map to visual observations of the area. After considering the 10 sol mission timeline and the outstanding objectives during "$N+$n" planning, the team decided not to land and conduct science activities in the smooth sediment area in favor of moving toward the younger lava.

On sol 102, the UAS Science Operations Team resumed its intended plan of investigating the older lava and sand sheet. The UAS conducted a mapping survey of the area between the landing site and the younger lava margin (Figure 3). The UAS landed on a sandy area between the younger lava margin and an outcropping of the older lava. Descent images of the sol 102 landing showed distinct areas of lighter and darker sediments (Figure 4(b)). The surface also showed a series of low-relief ripple or dune forms (approximately centimeter-scale amplitudes and meter-scale wavelengths; Figure 4(b)). A sample was taken on sol 103 using the scoop that included both lighter sediment visible on the surface and darker sediment exposed underneath (Figure 4(c)).

The sol 104 plan included oblique airborne images of the younger lava to characterize in detail the smoother and rougher surfaces identified in premission analysis (Figure 2(a)) and identify transitions between these textures that might indicate how the younger lava was emplaced. Images from the UAS revealed that the rougher texture was caused by heavily fractured thin plates of lava flow crust (Figure 4(d)), while the smoother texture was shown to be a more contiguous flow crust with sets of parallel lineations and long cracks (Figure 4(e)). The sol 104 landing site was chosen as the cache location for samples collected during the mission, and the sol 103 sediment sample was deposited here. Photos of outcrops of the older lava captured during sol 104 confirmed that these outcrops were too rough for a UAS landing, an operational constraint the UAS Science Operations Team had suspected based on premission

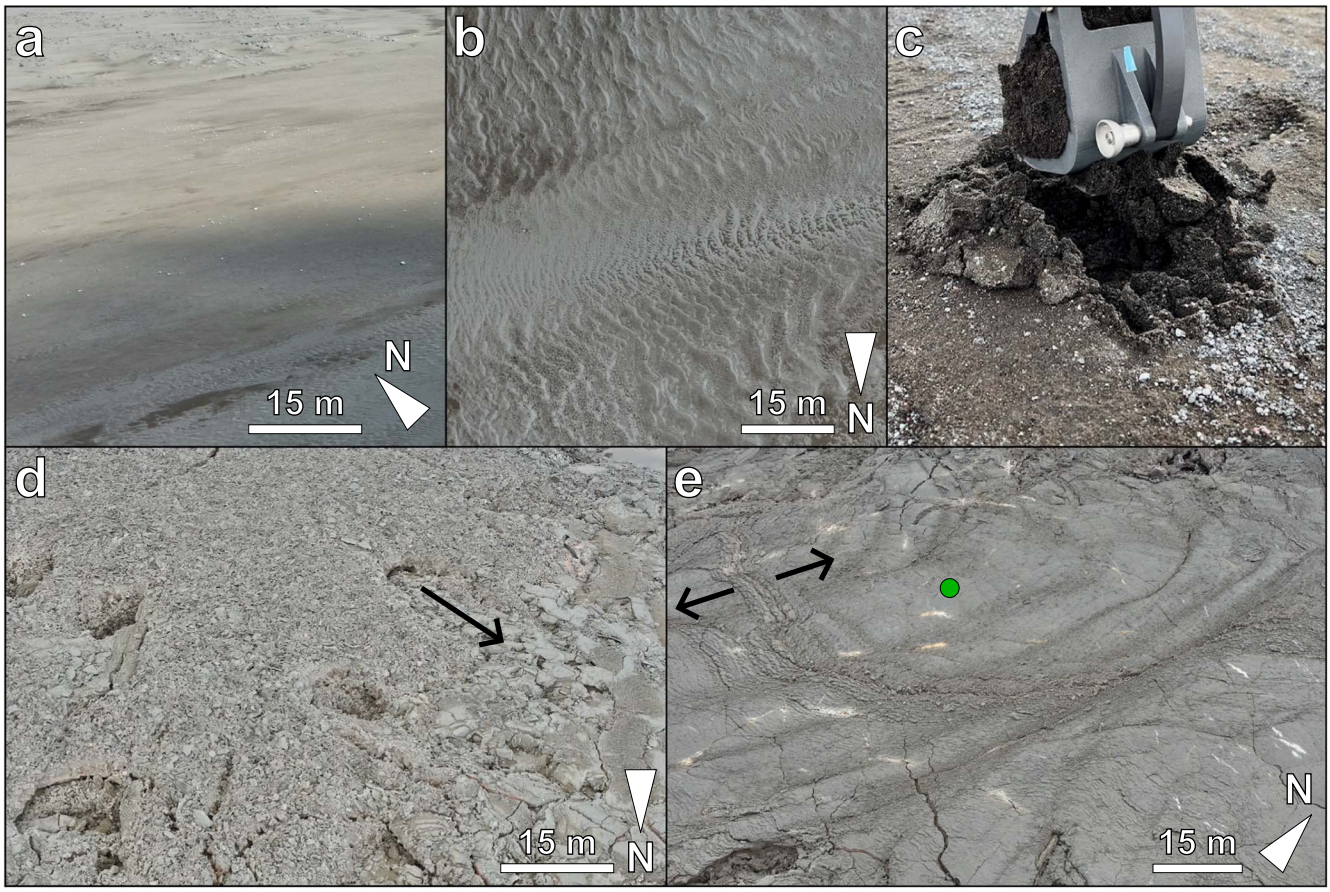

Figure 4. Surface textures in the UAS mission area. (a) Oblique image from sol 101 showing the smooth sediment surface in a topographic low scattered with light-toned boulders. (b) Nadir descent image showing the sol 102 landing area from an altitude of ∼40 m. Lighter and darker sediments are visible as part of a series of ripples. (c) The scoop sampler collects the sol 103 sample and exposes darker sediment beneath the surface. (d) Oblique image of the rougher surface of the younger lava from sol 104. The arrow shows the flow direction of a smoother texture lava breakout from the margin of a region of rougher texture. (e) Oblique image of the smoother surface of the younger lava from sol 104. The arrows show flow direction away from a crease structure located between the arrows. The green circle is the sol 105 landing site. All scale bars are approximate for the center of the oblique images. The scoop in (c) is ∼10 cm wide.

hazard analysis and images from sols 101 and 102. This would prevent the mission from sampling or conducting landed science on the older lava.

Photos from sol 104 were used to identify locations on the younger lava for two separate mapping surveys and a landing site on the lava itself. The mapping surveys targeted a location where the lava surface transitioned between the smoother and rougher textures and the lava landing site (Figures 2(a) and 3). The landing site was chosen because the sol 104 photos confirmed that it was the largest highly suitable area (Figure 2(b)) on the smooth surface of the younger lava that was accessible to the UAS Implementation Team. Both the mapping surveys and lava landing were executed during the sol 105 flight.

Sols 106–108 involved science activities on the younger lava surface. A sample of the lava was taken on sol 106. Descent and landed images from sols 105 and 106 showed that the lineations in the smooth lava surface texture (Figures 4(e) and 5(a)) were overlapping folds in the flow crust with a relief of tens of cm (Figure 5(b)). Microimages of the landing site showed a centimeter-scale roughness with sparse vesicles and slightly elongate, spinelike protrusions on the lava flow surface (Figure 5(c)). The $N+2$ plan for sol 107 created during the sol 105 planning meeting called for the UAS to conduct a short flight (∼10 m) and land on a surface with white discoloration to conduct landed science activities. However, upon review of the landed images from sol 105 (Figure 5(b)), the UAS Science Operations Team decided that the selected sol 107 landing site was not viable because the relief on the lava crust surface could cause the UAS to destabilize and crash during landing. Instead, the UAS conducted a short reconnaissance flight on sol 107, returning to land at the same location that it took off from. The surveys flown on sol 105 were also transmitted on sol 107. Using the sol 105 survey and images from sols 104 and 107, a suitable location to land on a white discoloration on the lava's surface on sol 108 was identified (Figure 5(d)). Premission analysis showed that these white discolorations were common in the immediate area (Figures 2(a), 3, and 4(e)) and were prioritized for observation by the UAS Science Operations Team for their potential to represent postemplacement mineral precipitation or alteration processes on the younger lava surface that could inform environmental conditions and the habitability potential of the area. The UAS flew ∼100 m to the chosen location, landed, and conducted landed science activities there on sol 108 (Figure 5(d)).

At this point in the mission, the UAS had collected images of targets on all four surface types identified premission and conducted landed science on two (Figures 2(a) and 3), achieving many of the mission science objectives (Table 1). The UAS Science Operations Team decided to prioritize two

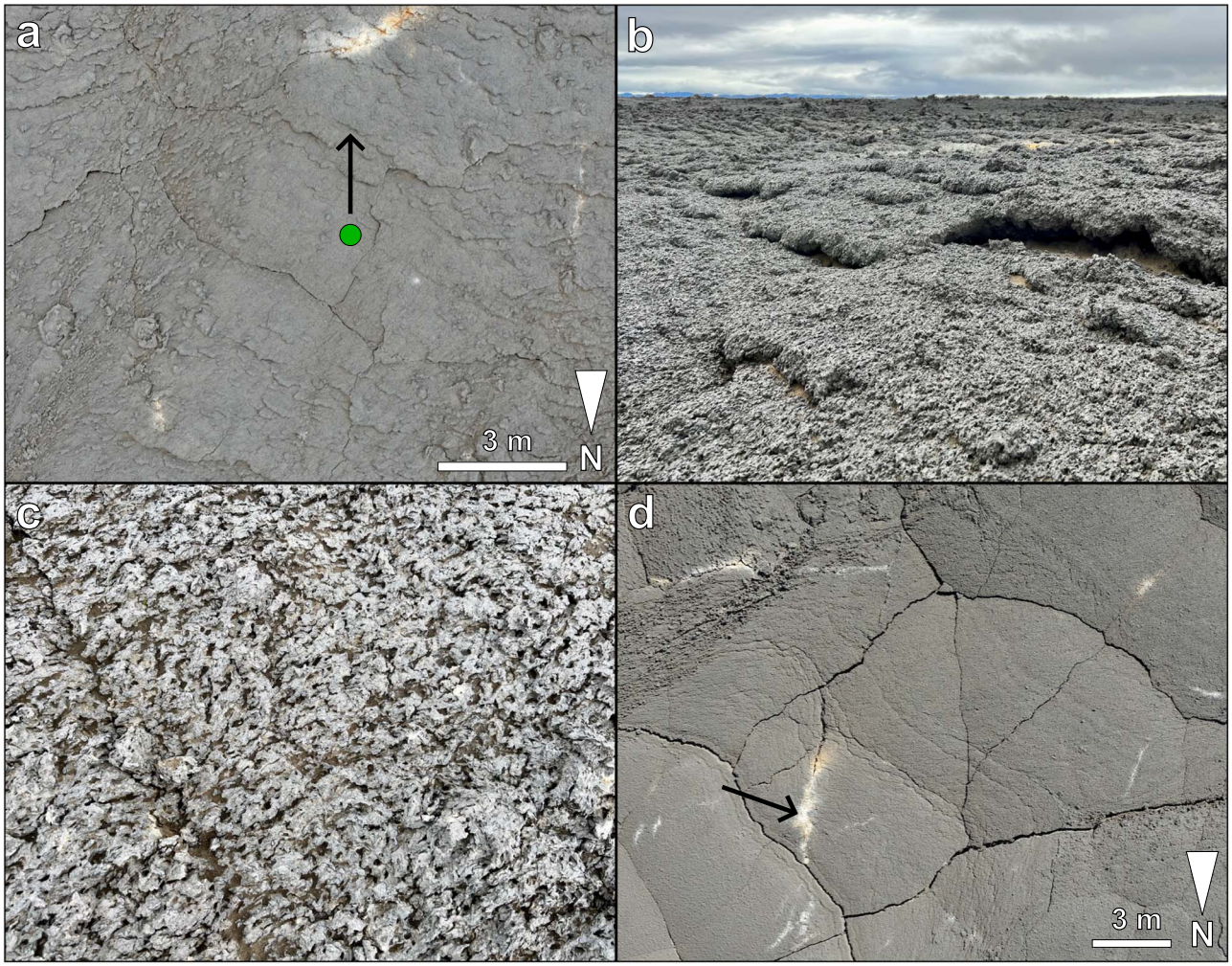

Figure 5. Lava landings sols 106–108. (a) Descent image of the sol 105 younger lava landing site (green circle) taken at an approximate altitude of 30 m. The arrow indicates the look direction of (b). (b) Landed image from sol 105 looking south and showing folds on the flow surface with relief of 10–30 cm. (c) Microimage of the younger lava at the sol 105 landing site. The image is ∼10 cm wide. (d) Ascent image from sol 109 taken at 40 m altitude showing the white discoloration where the UAS landed on sol 108 (arrow).

objectives during the remaining mission sols. The first would use airborne images to provide additional details on lava and sand sheet features cursorily identified in previous sols. The second would identify a location for the third sample and landed science that would help meet hydrology objectives, potentially by traversing further to the west or by returning to the smooth sediment plain surveyed on sol 101.

The UAS returned to the sample cache on sol 109 to deposit the sol 106 lava sample. Images taken on sol 109 aimed to further characterize the surface textures and topography between the younger lava margin and interior. These images and those captured on previous sols showed that the smooth surface was similar in appearance throughout the younger lava. However, the smoother surface in the interior was more expansive and located on a plateau-like topographic high (Figure 6(a)) compared to along the margin where the smoother texture was found on separate meter-scale flow lobes and broken by areas of rougher texture (Figures 6(a) and (b)). On sol 110, the UAS imaged older lava outcrops on the sand sheet to constrain observations from previous sols showing preferential accumulation of sediment on the east side of rock outcrops (Figure 6(c)). The UAS landed on a small marginal flow lobe on sol 110 (Figure 6(b)) to conduct landed science at a second location on the younger lava (landed science on sediment surfaces had already been conducted at three locations).

The UAS Science Operations Team had decided to end the mission by returning to the smooth sediment plain visited on sol 101 and collecting a sample to achieve the hydrology goal. Returning to this location was preferred over the western location because of the additional contextual information the team had already collected, the significant resources required to fly further west, and the smooth sediment plain's better proximity to the sample cache. However, due to incoming inclement weather at the field site, this plan was not possible for the UAS Field Implementation Team to execute in the time remaining. Instead, the UAS Science Operations Team opted for a more easily implemented plan where the third sample required by the mission goals was collected on the younger lava on sol 111, where the UAS had already landed on sol 110.

Sol 112 acquired oblique airborne images of a plateau in the younger lava interior where the surface was observed in the premission data to transition between the rougher and smoother surfaces (Figures 2(a) and 3). This target was important because more detailed images of the contact between these surfaces taken by the UAS could provide key observations to inform the emplacement history of the younger lava (Figure 6(d)). The UAS then flew back

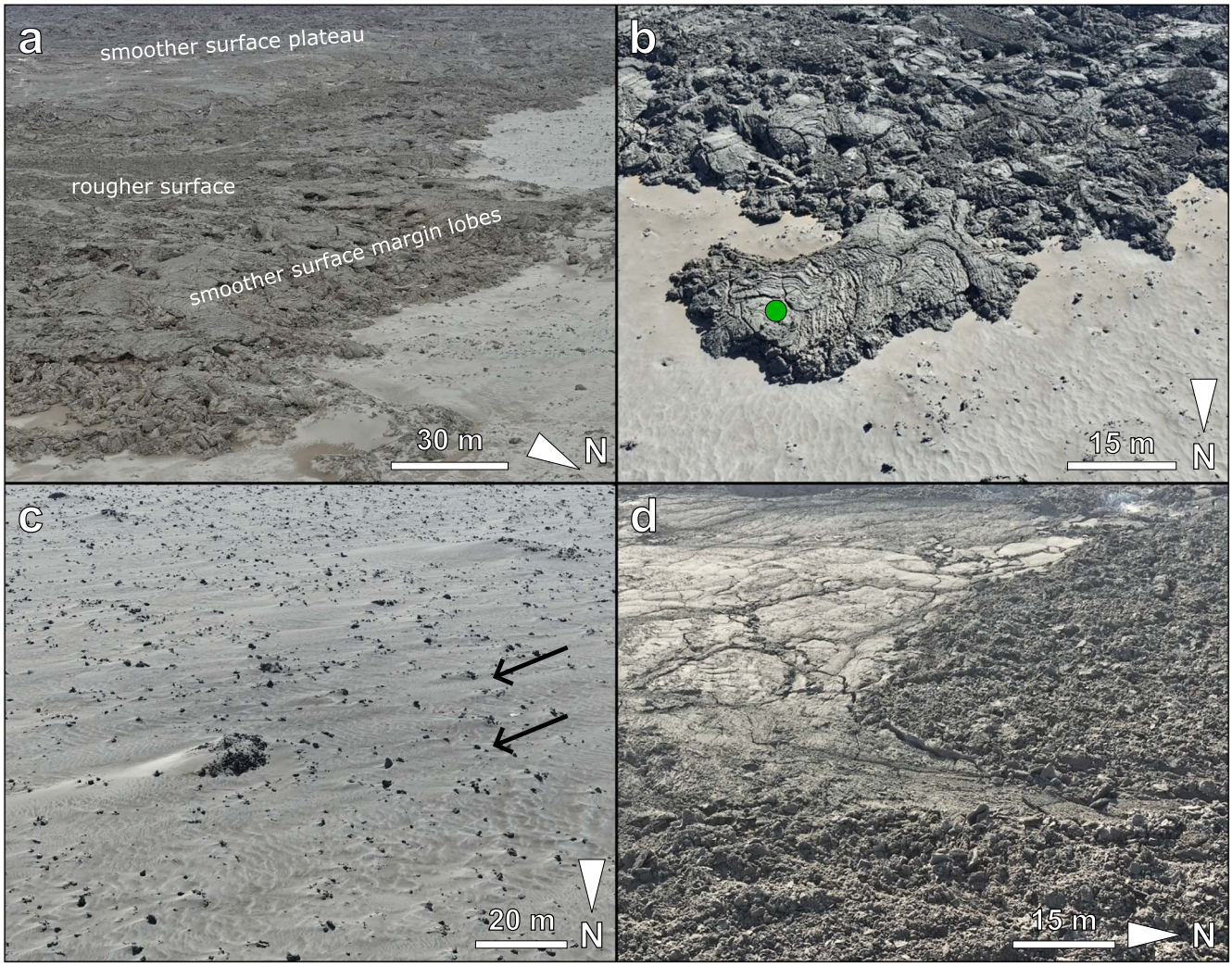

Figure 6. Observations from oblique images. (a) The younger lava interior is higher in elevation compared to the margin, and the smoother surface texture is also more continuous and extensive on the interior plateau compared to the margins. Rougher surfaces are located between the interior and margin. Image is from sol 104. (b) Smoother lava texture on a flow margin lobe where the UAS landed on sol 110 (green circle). Image is from sol 109. (c) Pockmarked terrain texture formed by blocks of the older lava protruding through the sand sheet. Sediment is preferentially deposited on the downwind side of larger outcrops, indicating a northeasterly wind direction (arrows). Image is from sol 101. (d) A transition between smoother and rougher texture in the younger lava from sol 112. All scale bars are approximate for the center of the oblique images.

to the east and landed at the sample cache to deposit the sol 111 sample. The simulated mission ended at this time after 12 sols.

4.2. Mission Data

In total, the UAS returned 86 images, nine LIBS measurements, nine VISIR measurements, and orthomosaics and DEMs from four surveys to the UAS Science Operations Team (Table 3). The UAS collected three samples, one of sediment and two of the younger lava (Figure 3). The images included 51 oblique in-flight images (e.g., Figure 6), 19 nadir images taken during ascent or descent (e.g., Figures 5(a) and (d)), nine landed horizontal images (e.g., Figure 5(b)), and seven images from the microimager (e.g., Figure 5(c)). Surveys covered a total of 70,000 m^2 and returned DEMs at 30 cm $pixel^{-1}$ resolution and orthomosaics at 6.0–9.6 cm $pixel^{-1}$ to fit within the UAS data budget. The resolution of the survey data represents an improvement by a factor of ∼3–4 for both the DEMs and orthomosaics over the resolution of the HiRISE-equivalent data provided to the Science Operations Teams prior to the mission (Figure 7).

The LIBS, VISIR spectrometer, and microimager collected data at each new landing site during the mission (sols 101, 102, 104, 105, 108, and 110). After each sample was collected (sols 103, 106, and 111), a second set of landed science measurements were taken. Landed science measurements were taken at four different geologic units or features: (1) the younger lava (sols 105, 106, 110, and 111), (2) a white discoloration on the younger lava (sol 108), (3) lighter sediment (sols 101, 102, and 104), and (4) darker sediment (sol 103). The darker sediment measurement was from the postsampling landed science on sol 103, where the sampling scoop exposed darker sediment beneath the lighter sediment on the surface (Figure 4(e)). VISIR spectra show general similarities between the four target categories and an absorption band at ∼1000 nm for relatively iron-rich silicate minerals common in basaltic lavas such as olivine and pyroxene (Figure 8). The differences in the width of this absorption between surface types may be due to differing abundances of olivine relative to pyroxene, variation in olivine and pyroxene composition, or the presence of glass (J. B. Adams et al. 1974;

Table 3
Operation Metrics and Summary of Data Collected during the UAS Mission

Sol	100[a]	101	102	103	104	105	106	107	108	109	110	111	112	Totals
Operations	…	…	…	…	…	…	…	…	…	…	…	…	…	…
Flight time (s)	…	252	257	0	221	295	0	64	39	191	123	0	230	1672
Flight distance (m)	…	1470	1052	0	1857	1370	0	146	93	1400	813	0	1800	10,001
Energy used (Wh)	…	333.1	330.4	330.8	310.2	330.6	330.8	124.9	97.2	251.5	199.4	330.8	300.7	3270.5
Data used (MB)	…	126.7	138.5	4.7	136.3	48.3	4.7	135.0	23.1	96.6	103.4	4.7	136.7	958.6
Percent power budget used[b]	…	99.9%	99.1%	99.2%	93.1%	99.2%	99.2%	37.5%	29.2%	75.5%	59.8%	99.2%	90.2%	…
Percent data budget used[c]	…	90.5%	98.9%	3.4%	97.4%	34.5%	3.4%	96.4%	16.5%	69.0%	73.8%	3.4%	97.6%	…
Data collection	…	…	…	…	…	…	…	…	…	…	…	…	…	…
Airborne oblique images	0	4	3	0	12	0	0	3	0	8	7	0	14	51
Ground images	2	0	2	0	1	2	0	0	0	0	0	2	0	9
Ascent images	0	0	0	0	0	0	0	0	0	1	0	0	1	2
Descent images	5	1	3	0	2	2	0	0	0	2	2	0	0	17
Microimages	0	0	0	1	1	1	0	1	1	0	0	2	0	7
LIBS targets	0	1	1	1	1	1	1	0	1	0	1	1	0	9
VISIR targets	0	1	1	1	1	1	1	0	1	0	1	1	0	9
Samples	0	0	0	1	0	0	1	0	0	0	0	1	0	3
Surveys	0	1	1	0	0	2	0	0	0	0	0	0	0	4
Survey area (m^2)	…	16,600	24,300	…	…	29,400	…	…	…	…	…	…	…	70,300
DEM resolution (cm)	…	30	30	…	…	30	…	…	…	…	…	…	…	…
Orthomosaic resolution (cm)	…	7.6	9.6	…	…	9	…	…	…	…	…	…	…	…
Orthomosaic resolution (#2) (cm)	…	…	…	…	…	6	…	…	…	…	…	…	…	…

Notes.
[a] Power and data calculators were not used for sol 100, when initial mission start images were downlinked.
[b] Power budget is 333.3 Wh sol^{-1}.
[c] Data budget is 140 MB sol^{-1}.

E. A. Cloutis & M. J. Gaffey 1991; R. G. Burns 1993; R. L. Klima et al. 2011). The clearest absorption present in the VISIR data is that of H_2O (1950 nm and the overtone band at 1450 nm) in the darker sediment from sol 103 and the white discoloration of the lava on sol 108 (Figure 8). The LIBS oxide data showed a basaltic-andesite composition with low alkali content and ~53% SiO_2 for all nine targets. However, we consider the LIBS measurements collected by the UAS Field Implementation Team to be unreliable, given that measurement error strongly correlated with measurement quantity, and there was no difference in measurements between the lava, sediment, and white discoloration on sol 108 (see the Appendix).

4.3. Mission Metrics

The UAS flew a total of 10 km over nine flight sols (Table 3; the other three sols were used for sample collection). The longest flight was 1857 m on sol 104, during which the UAS imaged a variety of different lava textures (Figure 3). The shortest flight was 93 m on sol 108, when the UAS flew from the sol 106 lava sampling location to the white discoloration on the younger lava (Figure 3). Total flight time was 28 minutes, with the longest single duration flight of 5 minutes on sol 105, during which the UAS conducted two separate mapping surveys (Table 3; Figure 3). The shortest-duration flight of 39 s occurred on sol 108.

The UAS used >90% of its 333.3 Wh power budget on eight sols (101, 102, 103, 104, 105, 106, 111, and 112) and transmitted >90% of the 140 MB data budget on five sols (101, 102, 104, 107, and 112) (Table 3; Figure 9). The UAS plan was energy-limited—defined here as no further activities could be included in the plan because there was insufficient power to do them—on five sols (101, 103, 105, 106, and 111), which included the three sols when a sample was taken. The UAS plan was data-limited—defined here as no further activities could be included in the plan because there were insufficient data remaining to transmit the results—on three sols (104, 107, and 112). On sol 102, the UAS plan was both data- and energy-limited (Table 3; Figure 9). On sols 108, 109, and 110, the planned activities were neither data- nor energy-limited. On one occasion, the UAS Science Operations Team circumvented the data limit by caching processed mapping survey data on the UAS at the end of one sol (105) and transmitting it on a later sol (107) that had minimal data acquisition and low power consumption.

Power was divided into "science" (operation of the instruments), "flight" (including takeoff and landing), "mapping surveys" (including flight, camera use, and processing time), "sampling" (use of the sampling apparatus), and "engineering" (data transmission, instrument start-up, maintaining vehicle temperature when not in use) categories (Table 2; Figure 9). Relatively long flights and mapping surveys used the most power (20%–64% and 38%–60% of daily cap; Figure 9(a)). Operation of science instrumentation (aside from sampling) used comparatively little energy (0.1%–2.4% of daily cap). Data volume was dominated by airborne images (11%–80% of daily cap; Figure 9(b)). On sols involving mapping surveys, substantial power (38%–60% of daily cap) and data volume (48%–72% of daily cap) were used on surveying, restricting any

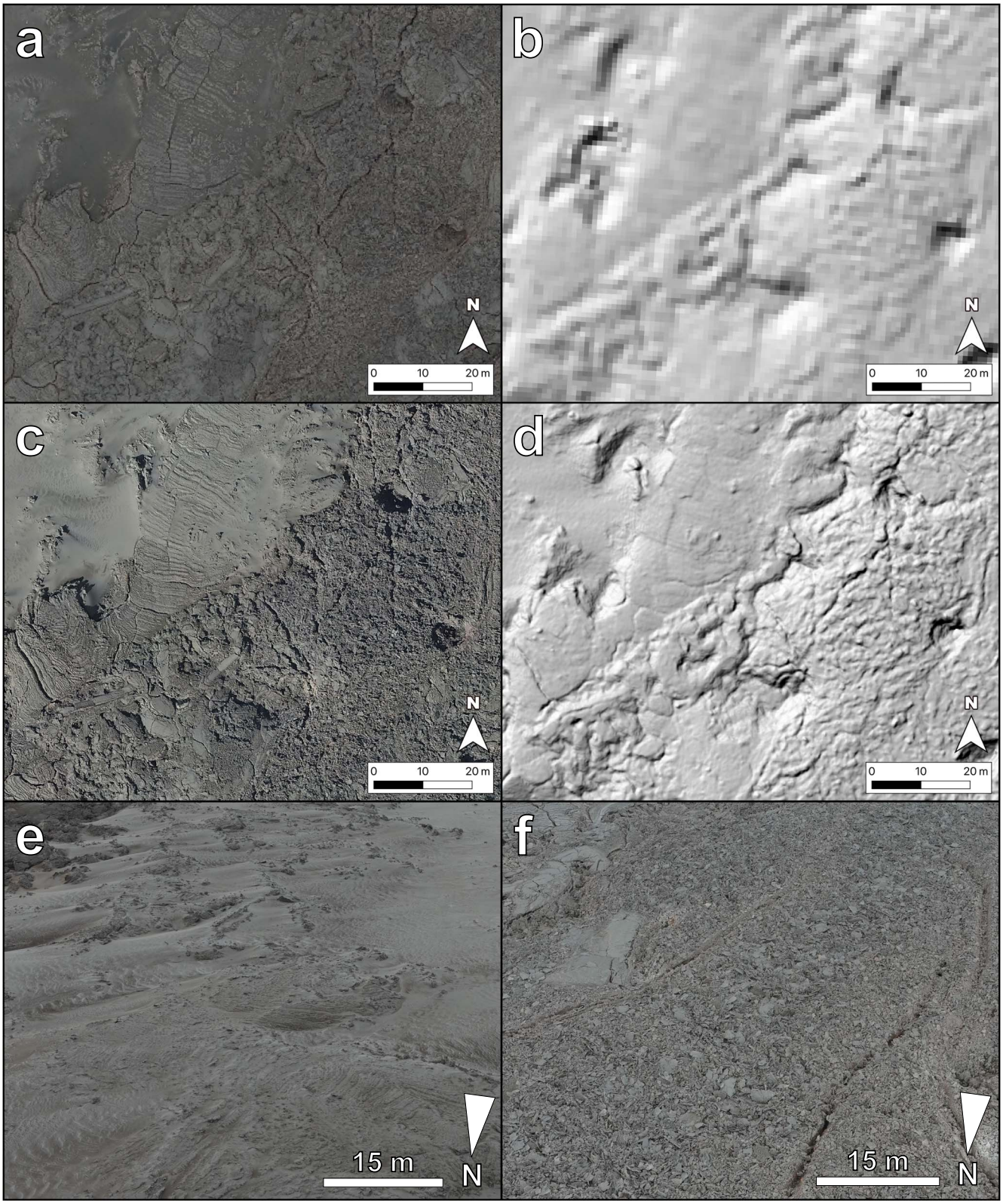

Figure 7. Resolution of analog orbiter and UAS mission data products. Surveys and images from the UAS mission significantly improved on the resolution of analog orbiter orthomosaics and DEMs. A location in the northern half of the UAS survey conducted on sol 105 near the sol 104 landing site (Figure 3) is shown in the (a) 0.25 m pixel^{-1} orbital analog orthomosaic, (b) 1.0 m pixel^{-1} orbital analog DEM, (c) 0.09 m pixel^{-1} UAS survey orthomosaic, and (d) 0.3 m pixel^{-1} UAS survey DEM. This location includes a rougher younger lava surface on the right side, a smoother younger lava surface in the upper center to lower left, and the sand sheet in the upper left. No oblique airborne images were taken by the UAS at this location, but similar terrain nearby was captured in images showing (e) the sand sheet mantling smoother lava in a sol 102 image at 40 m altitude and (f) the rougher lava in a sol 104 image at 60 m altitude. Scale bars in (e) and (f) are approximate for the center of the oblique images. Additional details observable in the UAS data (c)–(f) allowed for interpretations not possible with the orbital analog data (a)–(b) alone.

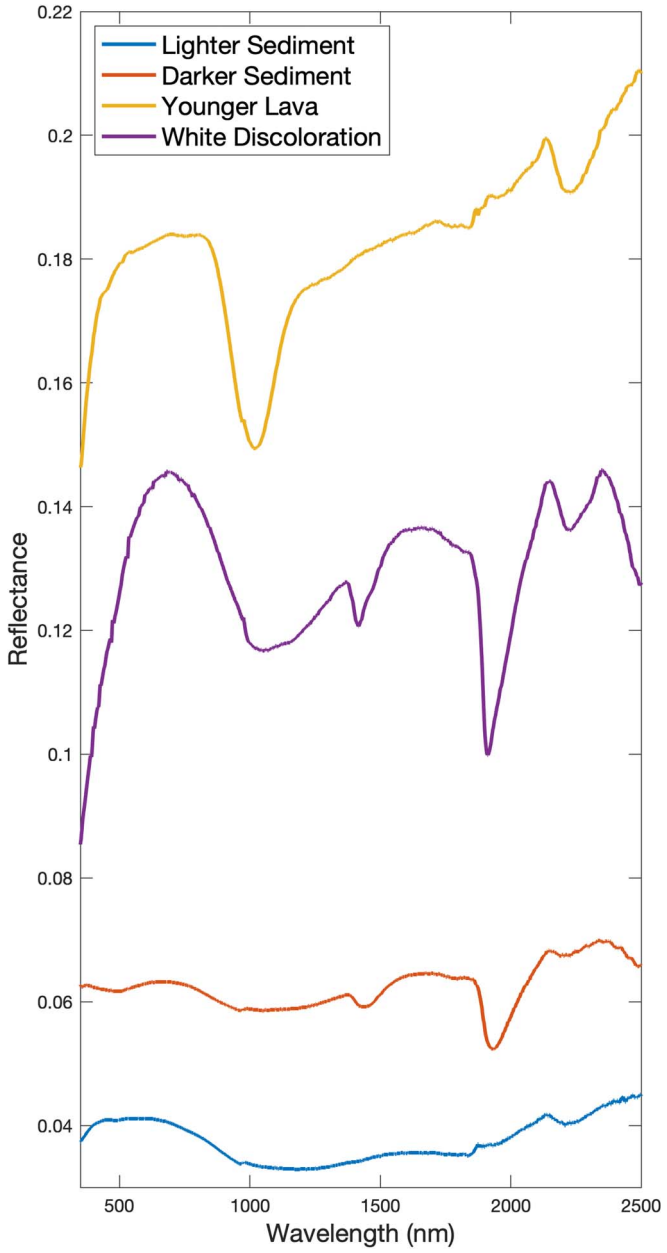

Figure 8. Point spectrometer data from the UAS mission. The VISIR spectrometer collected data on the lighter sediment (from sol 104), darker sediment (from sol 103), younger lava (from sol 111), and a white discoloration on the younger lava surface (from sol 108). The spectra show a broad absorption for basaltic minerals (olivine, pyroxene) at ∼1000 nm for all surfaces and a strong water absorption at 1950 nm and 1450 nm (overtone band) for the darker sediment and white discoloration. The reflectance in the *y*-axis for the darker sediment has been offset by 0.02 to improve figure clarity; the reflectance shown for the other three surfaces is the value measured by the instrument.

additional activities for that sol. Sampling also involved extensive power usage (84% of daily cap) and restricted additional activities on those sols.

4.4. Scientific Interpretation

Key science interpretations made by the UAS Science Operations Team using data collected during the UAS mission include the following.

1. The terrain with smooth sediment and dispersed light-toned boulders surveyed in sol 101 (Figure 4(a)) is a flood deposit, potentially a glacial outburst flood, or jökulhlaup, given the location's proximity to the nearby Vatnajökull ice cap (Figure 1).
2. The morphology of the younger lava was identified as "spiny" (or "toothpaste") lava (S. K. Rowland & G. P. L. Walker 1987), a transitional lava type indicative of emplacement of a relatively degassed lava at a slow rate. The plateaus and steplike topography of the younger lava suggests emplacement by a process of inflation and flow margin breakout of lava lobes.
3. The white discolorations on the younger lava are hydrated mineral precipitates from fumaroles. These features represent the best location identified by the UAS Science Operations Team during the mission to preserve biosignatures.

4.4.1. Sediments

The sediment in the mission area was generally well sorted with relatively few individual grains of pebble size (4–64 mm) or larger (Figure 4(c)). The lack of larger grain sizes or any obvious fluvial features such as channels strongly suggest that eolian-dominated transport was responsible for the formation of the features observed on the sand sheet. Wind ripples were ubiquitous across the surface of the sand sheet (Figure 4(b)). Ripple crests were generally oriented north–south or northwest–southeast and a few meters long with an intercrest spacing of ∼1 m. The amplitude of the ripples appears to be <10 cm in most cases, but the resolution of the DEMs from surveys on sols 101 and 102 was not high enough to confidently measure the topography of the ripples or identify the lee and stoss slopes that could suggest a transport direction. However, the UAS Science Operations Team observed accumulation of sediment preferentially on the northern to eastern sides of outcrops of the older lava in the area (Figure 6(c)). This suggests a predominantly northeasterly wind and transport direction. Supporting this interpretation is the orientation of the ripple crests (transport is perpendicular to the trend of wind ripple crests; N. Lancaster 1994) and the observation that west-facing margins of the younger lava have more sediment mantling than north- or east-facing flow margins.

Lighter and darker sediments were observed in both airborne and landed UAS images. Lighter sediment appeared to be located preferentially along ripple crests and in accumulations around outcrops of the older lava (Figure 4(b)). Darker sediment was generally located in ripple troughs and other topographic lows and was exposed beneath lighter sediment when the sampling scoop disturbed the surface on sol 103 (Figure 4(c)). The lighter sediment was characterized by a coarser grain size and poorer sorting compared with the darker sediment, which was finer-grained and well sorted (Figure 4(c)). VISIR spectra of the darker sediment showed absorption bands for water at 1450 and 1950 nm, suggesting hydration of these sediments (Figure 8). This suggests that the lighter sediment is the dominant sediment being transported by wind, while the darker sediment is held in place somewhat by moisture.

The smooth sediment plain in the northeast of the mission area targeted by the UAS on sol 101 is a flat depression that the

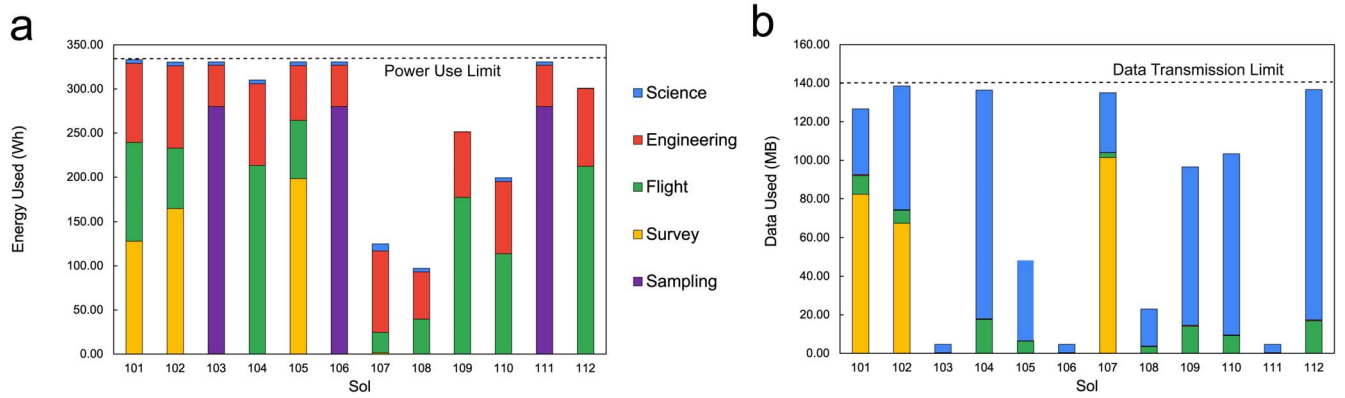

Figure 9. Resource usage during the UAS mission. The UAS activities for each sol were limited by both the power usage (a) and the volume of data that could be transmitted to the science team (b). These limits were often approached by UAS operations, with available power more frequently the limiting resource than data volume.

premission DEM shows to be ∼6 m lower in elevation relative to the higher standing older lava (Figures 2(a), 3, and 4(a)). Boulders were sparsely distributed through this area and appeared to have rounded surfaces in oblique airborne photos from the UAS (Figure 4(a)). The boulders averaged ∼0.3 m in diameter, measured using the 7.6 cm pixel^{-1} orthomosaic from the sol 101 survey (Table 3). Because the boulders appeared to be sitting on rather than protruding through the sediment, were lighter in color compared to the surrounding lava, and were found only in a topographic low, the UAS Science Operations Team interpreted this region to be a potential flood deposit and the boulders sourced from a location outside of the immediate mission area. A high-energy flood would likely have been required to form this deposit, as comparably sized boulders have been found in paleo-flash-flood deposits with flow rates estimated to be ∼500 m^3 s^{-1} (A. O. Clarke 1996; M. B. Baniya et al. 2019). In the analog orbiter orthomosaic, the smooth sediment plain was observed extending further to the east beyond the mission area, and a glacier is visible to the south (Figure 1), raising the possibility that the source of this flood was a glacial outburst jökulhlaup that covered a relatively large area. The potential evidence for glacial activity in the region also suggests glaciation as a source and formation mechanism for the large amount of sediment in the region.

4.4.2. Lava

During the premission analysis based solely on analog Mars orbiter data (Section 2.3), the younger lava was noted to have two primary surface textures: smoother and rougher (Figure 2(a)). The smoother surfaces in the interior had a polygonal fracture structure that was broken in places by a series of parallel lineations with seemingly random orientation (Figures 4(e), 5(d), and 6(d)). The interior smoother surfaces were also a topographic high, contained numerous pits, and were where the white discolorations were most common. Smoother surfaces were also present along the lava margin, where their appearance was more lobate. The rougher surface, which images from the UAS showed to be composed of thin, fractured crust plates (Figure 4(d)), was less prevalent and appeared intermixed with the smoother surface. Areas of rougher texture were generally located between the extensive smoother plateaus and the smoother lobate lava margin (Figure 2(a)). While the smoother surfaces appeared smooth in the premission analysis (Figure 2(b)), low-altitude oblique (Figure 4(e)) and landed images (Figure 5(b)) from the UAS showed these surfaces to have roughness on a scale that could impact safe UAS landings.

Observations from images taken by the UAS led the UAS Science Operations Team to interpret the younger lava in the mission area to be a "spiny" (or "toothpaste") lava type (S. K. Rowland & G. P. L. Walker 1987). This lava type is a transitional form of basaltic lava between the ʻaʻā and pāhoehoe end-members, and it forms during the emplacement of relatively degassed lava at slow rates (∼10–100 minutes m^{-1}; S. K. Rowland & G. P. L. Walker 1987). Once the lava has cooled, degassed, and become too viscous to form the typical smooth or ropey texture of pāhoehoe, the "spiny"' texture can form as long as the shear strain rates are low enough to prevent the lava's surface from ripping apart to form rubbly or blocky ʻaʻā textures (S. K. Rowland & G. P. L. Walker 1987). Parallel folded ridges and spines on the surface of the smooth plateaus that were observed in both airborne and landed UAS images (Figure 5) are diagnostic of the spiny lava type (S. K. Rowland & G. P. L. Walker 1987). Furthermore, the folds form perpendicular to the local flow direction, which allowed the UAS Science Operations Team to identify crease structures (S. W. Anderson & J. H. Fink 1992) where fresh lava emerged in a horizontal direction on the plateaus (Figure 4(e)). The variable orientation of the crease structures suggests that there was no dominant flow direction when the plateau formed. Evidence of lava emerging and flowing away from the base of higher-elevation flow regions (Figures 4(d) and (e) and 6(a) and (b)) suggests that the emplacement mechanism was dominantly one of inflation of the flow surface as lava continued to move into the area followed by squeeze-outs of spiny-textured lava from the margins of the inflating area, forming the smoother-textured lobes along the younger lava margin (Figure 6(b)).

The UAS Science Operations Team interpreted the white discolorations on the younger lava to be hydrated mineral precipitates from fumaroles. Observations from UAS images (both airborne and landed) showed that the white discoloration is a thin coating on the lava surface, and VISIR spectra showed hydration present in these features (Figure 8). The fumaroles formed where cracks in the surface crust allowed gases, dominated by water vapor, to escape the cooling lava. The volatile source driving fumarole formation was potentially moisture in the sediment over which the lava was emplaced. This is supported by the hydration also observed by the VISIR

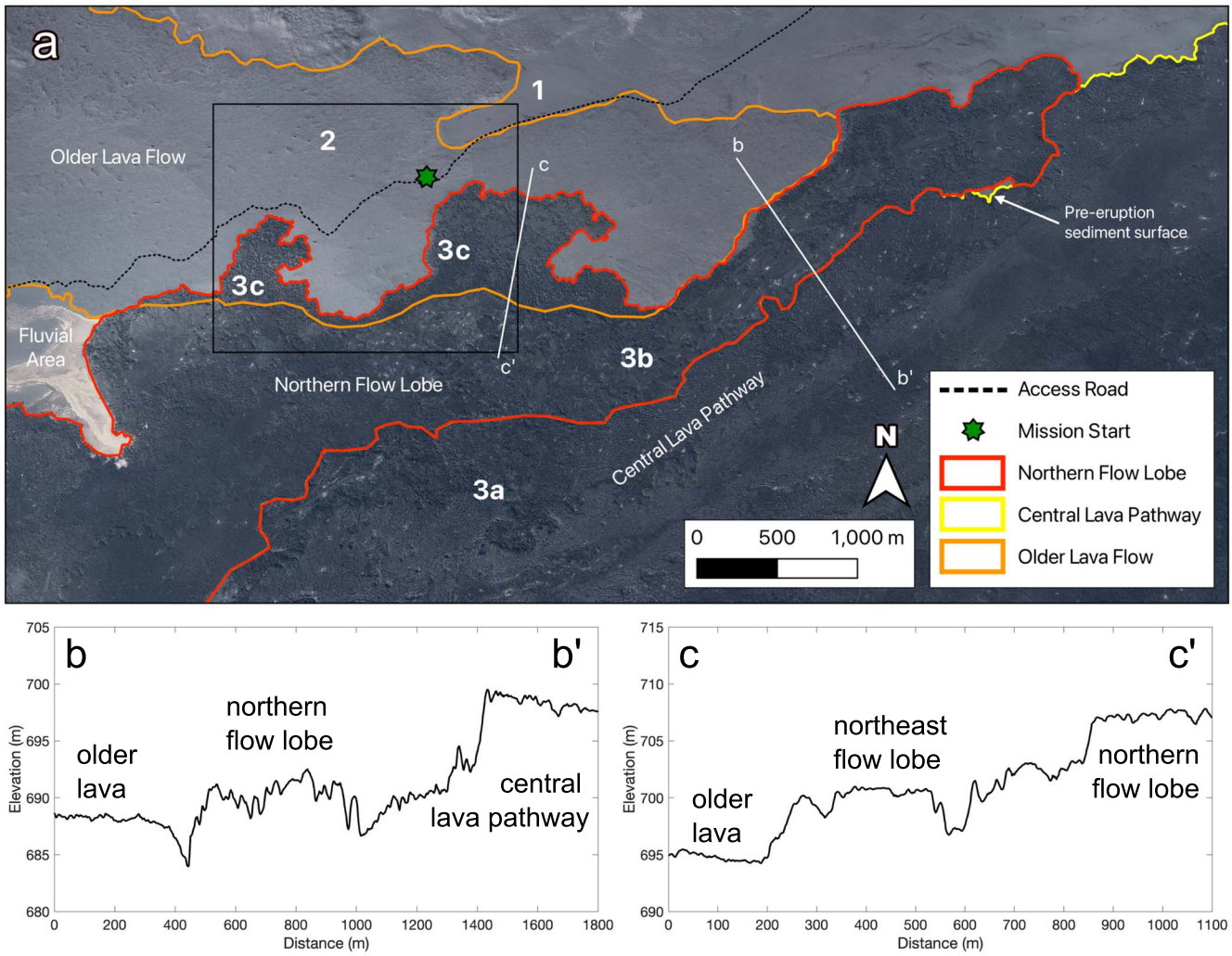

Figure 10. Geologic history of the mission area. The smooth sediment area (1) is the oldest unit in the mission area, followed by the older lava (2; orange outline). The central lava pathway was the first part of the younger lava flow field to be emplaced (3a; yellow outline) followed by the northern flow lobe (3b; red outline). The northeast and northwest flow lobes (3c) were the last parts of the younger lava flow field to be emplaced in this area, as the northern flow lobe inflated and overtopped the older lava. The sand sheet is the youngest surface, as transport of grains is ongoing. The sand sheet has been active since at least the older lava flow was emplaced, as the older lava flow was covered with sediment prior to emplacement of the younger lava flow. The black box in (a) denotes the extent of Figure 3. The white lines in (a) show the trace of the topographic profiles shown in (b) (b–b') and (c) (c–c').

spectrometer in the darker sediment and the uneven concentration of fumaroles on the surface of the younger lava.

4.4.3. Geologic History

The UAS Science Operations Team developed a geological history of the mission area using observations from the UAS mission and the analog orbiter data. The oldest unit observed during the UAS mission is the smooth sediment plain with dispersed light-toned boulders interpreted to be part of a widespread glacial outwash flood deposit (Figure 10(a)). As the boulders are not observed anywhere else, the most recent flood to affect the area likely occurred prior to emplacement of the lava. Next, the older lava was emplaced on top of the flood deposit. Analysis of the analog orbiter orthomosaic suggests that this lava is a flow sourced from the northwest, whereas the younger lava is part of a flow field sourced from the southwest (Figures 1 and 10(a)), suggesting that these lavas come from different volcanic systems. However, the UAS was not able to collect any geochemical data or samples from the older lava that would have enabled this interpretation to be tested more thoroughly. Eolian transport of sediment has been active at least since emplacement of the older lava (and likely much longer), as the older lava flow had significantly more sediment mantling its surface (to the point where interpretation of its morphology is not possible) than the younger lava.

Emplacement of the younger lava flow field is interpreted to have begun with its central pathway, located ∼1 km south of the mission area (Figure 10(a)). The lava observed by the UAS during the mission, referred to now as the northern flow lobe, was emplaced later from a source to the southwest near the vent, perhaps a levee failure or change in vent location or geometry that led lava to stop flowing down the central pathway and be redirected into the northern flow lobe. These interpretations are supported by observations in the analog orbiter orthomosaic and DEM of a trough between the northern flow lobe and the central pathway that includes gaps showing the preeruptive sediment surface between these flows (Figures 10(a) and (b)). A smaller trough is located between the northern lobe and the older lava (Figure 10(b)), suggesting that the northern lobe was emplaced in a topographic low between the older lava flow margin and the central pathway of

the younger lava flow field. Furthermore, the two smaller northward-extending flow lobes that were the focus of the UAS mission have lower elevations than the northern lobe (Figure 10(c)). This topographic break trends east–west and appears to follow the boundary of the older lava flow and a fluvial area (orange line; Figure 10(a)). It is likely that these northernmost lava lobes formed only after the northern lobe rose above the older lava, allowing lava to break out from the inflation plateau and inundate the area. Thus, the younger lava surface investigated during the UAS mission may represent one of the final stages of emplacement during the eruption that formed the younger lava flow field.

The fumarolic deposits on the flow surface are concentrated on smoother surfaces of the younger lava flow-field plateau and are not found in the northernmost lobes. Much of the younger lava flow field, including the plateau, was potentially emplaced above a fluvial system that followed the south margin of the older lava flow, visible to the west of the younger flow in the analog orbiter orthomosaic (Figure 10(a)). The presence of lava above water may explain the concentration of fumaroles in this area and the lack of fumaroles in the northernmost lobes that were emplaced above the older lava flow, which presumably held less moisture.

Knowing the lava type and the width and thickness of the northern lava lobe (Figure 10(b)), the UAS Science Operations Team estimated the emplacement parameters for the younger lava flow field. S. K. Rowland & G. P. L. Walker (1987) show that spiny lava is emplaced at a flow rate of 10–100 minutes m^{-1}. The cross-sectional area of the northern lobe at the cross section location in Figure 10(b) is 2700 m^2. This results in a rough estimate of the eruption rate of ~3 $m^3 s^{-1}$ during emplacement of the northern lobe. The entire younger lava flow field has a surface area of ~80 km^2. Extrapolating from the elevation of the ground next to the flow margins suggests that the lava may have an average thickness on the order of ~20 m; thus, the flow field may have a bulk volume of ~1.6 km^3. Applying our 3 $m^3 s^{-1}$ effusion rate estimate to the entire eruption—a major assumption—gives an eruption duration on the order of ~15 yr. Given that eruption rates often peak in the initial phases of an eruption at orders of magnitude greater than rates observed in the waning phase of an eruption (G. Wadge 1981), and this extrapolation ignores the possibility of multiple flow lobes being emplaced simultaneously, this duration estimate was considered to represent a maximum value. We note here that the main phase of the 2014–2015 Holuhraun eruption actually lasted for only 180 days (i.e., from 2014 August 31 until 2015 February 27; E. Bonny et al. 2018).

4.4.4. Astrobiological Implications

Determining the habitability of the mission area was a key component of the science objectives for the UAS mission (Table 1), which were based on priorities in planetary science guiding documents (MEPAG 2020; National Academies of Sciences, Engineering, & Medicine 2023). However, because this analog mission took place on Earth, the study area is fundamentally habitable. Consequently, our interpretations of the habitability of the region must be taken in context, since even the most extreme environments on Earth are likely optimistic end-members in terms of habitability for any potential habitat on Mars or other planets.

The likely presence of fumaroles on the younger lava flow surface, as indicated by the white mineral deposits, represents a location with high potential for biosignature preservation (A. L. Brady et al. 2020). Fumaroles can be islands of habitability in extreme environments (E. K. Costello et al. 2009) and can potentially carry biosignatures from subsurface environments to the surface (N. Hadland et al. 2024). However, further geochemical analysis would be required for confirmation of the origin of these deposits and their potential for habitability. Evidence for hydration within the darker sediment combined with the possible lack of transport of this sediment could suggest a stable near-surface habitat within the sand sheet. Similar near-surface habitats that undergo desiccation processes can have microbial communities that are preserved until another rewetting event occurs and they are reactivated (D. Schulze-Makuch et al. 2018).

5. Discussion

5.1. Premission Planning

Analysis of the orthoimages (0.25 m $pixel^{-1}$) and DEMs (1.0 m $pixel^{-1}$) of the mission area prior to implementation was crucial to mission success. These data were essential for mapping UAS landing suitability (Figure 2(b)), identifying the main surface units and their characteristics (Figure 2(a)), and creating initial hypotheses to test during the mission. The change in the mission start location from a site further west to the implemented location further east impacted the efficiency of the initial sols of the UAS mission. During premission planning, the UAS Science Operations Team had prioritized targets to the west and created tentative plans for the initial mission sols based on the assumption of this starting location (Figure 2(a)). When the start location changed (Figure 3), the team was less familiar with that area and had to perform additional work to identify potential targets concurrently with planning the UAS activities. A preferred and commonly implemented strategy for missions (but not performed by the UAS Science Operations Team here) is to map contacts between geological units and facies to identify regions of interest over a larger area rather than only identifying specific targets.

5.2. Instrumentation and Data

5.2.1. Images

Oblique airborne images captured by the UAS (e.g., Figure 6) were the most useful type of images collected for mission planning and interpretations. The oblique look angle enabled perception of depth of field with foreground and background elements. For the UAS Science Operations Team, this made understanding the relief and roughness of the surfaces easier compared to the nadir perspective of the analog orbiter and mission survey-derived orthomosaics, allowing for more confident interpretation of features in the image. The oblique airborne images were also taken at lower flight altitudes compared to the mission surveys, making the oblique images the highest-resolution airborne image data available to the UAS Science Operations Team (Figure 7). Notably, the oblique images were used to confirm the suitability of UAS landing areas for future sols that had been tentatively identified using the hazard map (Figure 2(b)). In contrast, nadir images (Figures 5(a) and (d)) were less helpful individually because of the self-similarity of the terrain (particularly over the sand

sheet), and the viewing angle made it difficult to resolve differences in relief.

We found that using the same look angle and altitude for airborne oblique images (40° from horizontal at 60 m above ground level for most flights) was helpful, as the perspective remained the same while the terrain changed, which assisted with comparing different surfaces. Ground sampling distance (i.e., pixel size or image resolution) can be estimated based on look angle, altitude, and the camera's field of view, but this was complicated during the simulated UAS mission by our use of GNSS to control flight altitude, which left unknown the elevation variations of the surface at the scale of the image resolution. This highlights the need for future camera system designs to be integrated with laser rangers to determine (1) the height of the UAS above the ground surface at all times (Ingenuity included a laser altimeter for this purpose; J. Balaram et al. 2021) and (2) distances to features in oblique images to more effectively calculate scale.

Ground-based and microimages were at times crucial for mission planning. For example, images from sol 105 (Figures 5(b) and (c)) motivated the UAS Science Operations Team to modify their initial plans for a second lava landing on sol 107 and instead used sol 107 to scout for a site to land on sol 108 (Section 4.1). However, many ground-based images returned to the UAS Science Operations Team were of poor quality (e.g., out of focus or over-/undersaturated because of the contrast between the dark surface and the bright horizon), limiting the use of these images for mission planning and interpretation. This emphasizes the importance of considering factors such as camera focal length, camera look angle and azimuth, and illumination angle when selecting ground-based image targets. The microimager was useful for identifying fine-scale features on the ground such as vesicles in the lava or the approximate sizes of coarse grains (Figures 4(c) and 5(c)).

5.2.2. Photogrammetric Surveys

Photogrammetric surveys to create the 30 cm pixel^{-1} DEMs and 6.0–9.6 cm pixel^{-1} orthomosaics (Table 3) were most useful for postmission scientific analysis. At the flight altitudes and export resolution chosen by the UAS Science Operations Team, survey map products represented a threefold-to-fourfold improvement over the 1.0 m pixel^{-1} DEM and 0.25 m pixel^{-1} orthomosaic data sets intended to simulate the resolution of data from HiRISE (A. S. McEwen et al. 2007; S. S. Sutton et al. 2022; Figure 7). Higher-resolution products were possible if the UAS Science Operations Team had chosen to fly surveys at lower altitude and devote more resources to transmitting the data. Survey products were used to measure boulders in the smooth sediment plain (Figure 4(a)), ripples throughout the sand sheet (Figure 4(b)), and various morphological features on the younger lava surface (Figures 4(d) and (e)).

Conducting surveys, however, used significant power and data that severely limited other activities the UAS could perform and how far the UAS could travel from the takeoff location (Table 3; Figure 9). Performing regular surveys during the mission to complete a large contiguous mapped area, as was initially proposed as a mission plan (Figure 2(a)), was deemed not the best use of resources. Instead, after conducting surveys on sols 101 and 102, the UAS Science Operations Team decided to limit surveying to only targets where the high-resolution data could potentially provide diagnostic information that oblique airborne images could not. Only two more surveys were conducted during the rest of the mission, both on sol 105, targeting (1) a transition between the smoother and rougher lava textures and (2) the lava surface where the UAS landed on sol 105 (Figure 3). For mission operations, oblique airborne photos provided less quantitative information relative to the surveys but were more resource-efficient for quick identification of future targets and landing sites. The surveys could have proven more useful had the UAS Science Operations Team been able to plan more carefully the extent and scale of the desired products. For example, a survey could have been modified to ensure that the sediment ripples would be resolved in the DEM, allowing for more detailed measurements of the features. Planning duration limitations (Section 3.2) prevented this calculation, but modification could be feasible on a typical Science Operations Team with additional personnel in specified roles.

5.2.3. Landed Science

The ability of the samplers to disturb surfaces proved to be useful in concert with other instruments. For example, VISIR measurements showed hydration when targeting darker sediment newly exposed by the sampler (Figures 4(c) and 8). Using the sampler consumed nearly the entire power budget of the UAS for a given sol, meaning that minimal other activities could be performed during the same planning and data-acquisition cycle (Figure 9). This is likely not a hindrance for longer missions, where a UAS may have multiple sols to recharge its batteries, conduct landed science, and downlink data, but for this 12 sol simulation, spending three sols stationary to perform sampling greatly limited the potential area covered by the UAS. For a UAS mission designed to collect multiple types of data while exploring a large area in pursuit of multiple science goals, the use of a sampler and then transporting and dropping the samples in a cache on the surface is likely not an efficient use of resources. Including the ability for a future MSH to abrade/disturb and measure, but not sample, a given surface may reduce the complexity of the mission design while enabling valuable observations of fresh surfaces using other science instruments. For missions where acquiring samples via UAS is the top priority, the UAS should be designed for that specific purpose and not expected to perform other complex science activities.

The LIBS and VISIR spectrometer both made significant contributions to the mission by collecting data that informed important interpretations while using relatively little energy and few data resources. The VISIR data were essential for recognizing hydration within the sediment and white discoloration on the younger lava surface. However, issues with the measurement consistency and error of the handheld LIBS used by the UAS Field Implementation Team (Section 4.2) prevented the UAS Science Operations Team from making more detailed interpretations with LIBS data beyond noting the broadly basaltic composition of all materials measured.

The most significant limitation to the use of the landed science instruments during the RAVEN UAS mission was that instruments were statically mounted to the UAS to observe a target directly underneath the vehicle. The consequence of this design is that the UAS was only capable of science observations at surfaces on which it had landed. This resulted in the UAS mission not being able to collect a sample, geochemical data, or microimages of the older lava, limiting the scope of interpretations the UAS Science Operations Team

could make concerning this unit. Future mission simulations and MSH designs would benefit from the development of a robust landing capability (e.g., R. Brockers et al. 2021) and/or a pointable robotic science arm (e.g., C. Rutter & M. Lach 2022). These capabilities would enable landed science instruments to have more targeting flexibility by allowing landings on rougher surfaces and targeting of features from a distance of a few meters while landed. Targeting of features a few meters from the vehicle is accomplished in part via a robotic arm on the Curiosity and Perseverance rovers (J. P. Grotzinger et al. 2012; K. A. Farley et al. 2020), and a robotic arm has been proposed for a future MSH (C. Rutter & M. Lach 2022).

5.3. Operational Decision Making

The UAS Science Operations Team developed a "reconnaissance-then-science" strategy, where they planned a long flight to capture as many images ($\sim$15 sol^{-1} given the image resolution and data limit) of as many sites of interest as possible over a large area. The images from this flight were used to identify the optimal locations to target on subsequent sols for a mapping survey, landed science, and/or landing. This strategy is shown in practice on sols 104–108 of the UAS mission (Figure 3). The long sol 104 flight allowed the UAS Science Operations Team to identify areas to survey and land on sol 105, sample on sol 106, and conduct landed science on sol 108. This strategy combines the positive aspects of both covering a large area with sparse observations for context and conducting activities at select targets for in-depth investigations. Reconnaissance flights improve mission safety by confirming landing suitability and increase scientific return by helping identify ideal locations for surveying and landed science. This strategy is conceptually similar to the "walkabout" strategy tested by R. A. Yingst et al. (2020) for rover operations and preferred over a "linear" approach for similar reasons discussed here; the "walkabout" approach provided more regional context and greater confidence in interpretations. Applying a "walkabout" strategy is potentially even more advantageous for UAS operations (or joint rover–UAS operations), as the UAS can acquire the contextual information faster compared to a rover, likely using a single flight at relatively high altitude to capture airborne images of a large region of interest.

The "reconnaissance-then-science" strategy also worked well with the mission constraint that the UAS return to a cache location after collecting each sample. The "tethering" of the UAS to a central location allowed for retargeting of features from different perspectives or detailed targeting of new features of interest identified in downlinked images and contributed to a greater understanding of the geology of the mission area. The requirement to cache samples was among the rationale for the UAS Science Operations Team's decision to favor focused investigations at high-priority locations, as opposed to a "linear" approach to maximize UAS flight distance, which was discussed during premission planning. For a longer mission, a cache requirement would impose a more significant constraint on the ability of the UAS to cover terrain, and the Science Operations Team would have to prioritize between collecting more samples in the immediate area (if the sampler design allowed for more samples) and exploring new terrain further away.

Flexibility in altering intended sol plans was essential for achieving mission success. The revised planning during sols 107–108 highlights a case where our landing suitability mapping (Figure 2(b)) and oblique image scouting were insufficient to identify potential hazards. The steplike topographic breaks created by the folds in the spiny lava texture (Figure 5(b)) were averaged out across the 1.0 m pixel size of the DEM, and the airborne images from sol 104 only viewed the landing site from one direction, where the relief was difficult to discern (Figure 4(e)). This example demonstrates that subpixel-sized relief can impact UAS operations even when the pixel size is of similar or smaller dimensions relative to the vehicle itself. Mitigation of the risk posed to UAS landings by smaller-scale but sharp topographic relief can involve three components. First, scouting of landing sites during previous sols should include viewing potential landing zones from multiple directions and altitudes. Second, prior characterization of the surface unit where a landing is proposed will help identify on which surface types hazardous small features are more likely to exist. Third, the UAS should be equipped with both an autonomous landing site selection system (e.g., R. Brockers et al. 2021) and robust landing gear capable of adapting to any surface features too small to be detected at the resolution of the data available to the Operations Team.

5.4. Science Return of the UAS Mission

Data collected by UAS were essential to developing an interpretation of the area's geology at the level of detail described in Section 4.4 The analog orbiter orthomosaics and DEMs provided prior to the mission simulation provided an initial characterization of the terrain and guided the development of hypotheses to test during the mission but could not resolve the details or provide data types that led to the key science conclusions of the mission (Section 4.4). For example, it was not possible to determine the spiny lava type of the younger lava from the analog orbiter data. However, the higher-resolution images and surveys from the UAS (Figures 6 and 7) were able to observe the diagnostic features (Section 4.4.2; Figure 6) that led to this interpretation. The emplacement conditions of spiny lava are significantly different from those for ʻaʻā and pāhoehoe lava types (S. K. Rowland & G. P. L. Walker 1987); thus, this interpretation made possible by UAS data had significant implications for the UAS Science Operation Team's understanding of the formation of the younger lava flow field.

Data from the UAS mission helped confirm, elaborate on, or explain observations and hypotheses from the analog orbiter data. The possible interpretation of the white discolorations as mineral precipitates was identified during premission planning, but UAS images were needed to confirm that the color was a coating on the lava surface and the UAS VISIR spectrometer provided observations of a composition different than that of the lava with evidence for hydration (Figure 8). The identification of these features as fumaroles on the lava surface was the most significant mission finding related to astrobiological studies and implications for habitability. Similarly, the improved resolution of the UAS surveys and images (Figure 7) allowed the UAS Science Operations Team to measure boulders in the flood deposit and wind ripples on the sand sheet. This analysis was not possible given the resolution of the analog orbiter data and helped confirm premission hypotheses for these terrains and add detail to the interpretation of their formation. The analog orbiter orthomosaics and DEMs were

Table 4
Surfaces Targeted by UAS Instruments

	Airborne Oblique Image	Photogrammetric Survey	Microimage	LIBS	VISIR	Sample
Smooth sediment	Yes	Yes	No	No	No	No
Pockmarked terrain	Yes	Yes	Yes	Yes	Yes	Yes
Older lava	Yes	Yes	No	No	No	No
Younger lava—smoother	Yes	Yes	Yes	Yes	Yes	Yes (2)
Younger lava—rougher	Yes	Yes	No	No	No	No
Younger lava—white discoloration	Yes	Yes	Yes	Yes	Yes	No

the main sources for interpreting the region's geologic history (Section 4.4.3; Figure 10), but details from UAS observations provided supporting information that improved the UAS Science Operations Team's confidence in their conclusions.

5.5. Assessment of Mission Success

The UAS successfully completed a 12 sol mission and collected three samples, as required in the mission guidelines (Section 2.2). The UAS was able to achieve the science objectives outlined in the STM (Table 1) while following the operational and implementation limitations (Section 2). The detailed interpretation of data collected during the mission (Section 4.4) addressed at least in part all four of the key questions identified by the UAS Science Operations Team prior to the mission (Section 2.3) and constructed a geologic history of the area (Section 4.4.3). Every major surface texture in the area identified premission by the Science Operations Teams was captured in oblique airborne images and mapping surveys (Table 4). However, only the pockmarked terrain and smoother surface of the younger lava were targeted for landed science, as the other units were too rough for the UAS to land on. Three of four sample targets were achieved. Samples of the sediment (on sol 103) and younger lava (on sols 106 and 111) were collected, and, as a hydration signal was detected at the location of the sediment sample, this sample also accomplishes the hydrology objective (Table 1; Figure 8). No sample of the older lava was collected.

The greatest hindrance to further mission achievements were "testisms" imposed by the brief duration of the simulated mission and inclement weather encountered in the field, as well as limitations in personnel. Time constraints during mission implementation motivated the UAS Science Operations Team to continually move on to new areas to achieve all mission objectives and increased the consequences of small inefficiencies in the mission plan. For example, the team chose not to conduct landed science activities in the smooth sediment plain on sols 101 and 102 in favor of moving toward the younger lava, and the mission simulation ended before the UAS could return to this location to collect a sample. Although the size of the UAS Science Operations (four people) and Implementation (six people) Teams was appropriate for the tasks of creating and executing the UAS plan for each sol (Section 3.1), the UAS Science Operations Team would have benefited from a greater breadth of scientific expertise. The team lacked expert knowledge related to sedimentology and glaciology, which would have helped to inform the selection of science targets on the sand sheet and interpretations of the mission data. Additional Science Operations Team support would have enabled more data analysis during the mission (e.g., calculation of image ground sampling distances) and more precise mission plans (e.g., ensuring that the resolution of surveys would resolve key details at science targets).

UASs offer numerous advantages for exploring terrain in the Holuhraun region of Iceland. The broad homogeneity of the terrain, with contacts between different surface units spaced hundreds of meters apart (Figure 2(a)), and the variable roughness of these units (Figure 2(b)) makes traversing the area time-consuming and hazardous on the ground. The UAS was able to travel relatively large distances in short amounts of time (e.g., on sol 104, the UAS covered 1857 m during a flight lasting 3 minutes and 41 s; Figure 3 and Table 3) and bypass rough terrain by flying over it. This capability enabled the UAS Science Operations Team to characterize multiple surface types (Table 4) in a region of $\sim$1 km^2 during a short 12 sol mission.

6. Conclusions

We conducted a simulated Mars surface exploration mission spanning 12 sols using a UAS. The mission was planned to resemble initial designs for an MSH (J. Bapst et al. 2021) and assess the capabilities and operational strategies best suited for a planetary UAS mission. The UAS used oblique airborne imaging, mapping surveys, sampling, and geochemical instrumentation to explore a Mars analog terrain at Holuhraun in the Icelandic highlands. The mission succeeded in achieving operational goals of a duration of 10 sols or more while collecting and caching at least three samples. The mission collected one sample from the sediment and two from the younger lava, with the sediment sample doubling as a hydrologic sample. A sample of the older lava was not collected. We characterized the chemistry and surface morphology of much of the terrain observed and developed a detailed geologic history of the region.

The design, planning, and implementation of the RAVEN UAS mission led to several lessons learned and the development of operational strategies for conducting a planetary UAS mission. Our key conclusions are as follows.

1. A UAS is an ideal planetary exploration vehicle when the goals of exploring a region require traversing large distances, especially if the area consists of rough or steep terrain that would limit the ability of ground-based exploration (e.g., via rover and/or human) to access regions of interest safely and within a reasonable time frame.
2. Oblique airborne images were the most important data type for mission planning and scientific analysis. Similarity in perspective and scale was important for comparing surfaces between images. We preferred a look angle of $\sim$40° and recommend that future camera systems be integrated with laser rangers to improve quantification of surface scale. Although photogrammetric surveys were useful for detailed postmission

analysis of targets (e.g., sediment ripples or lava morphology transitions), their resource cost made them impractical for operational or frequent use.

3. Landed science, including geochemical and submillimeter-scale image observations, was essential to provide detailed morphological and compositional information that can be integrated with the regional context enabled by airborne images. Yet our UAS design could not land on rougher surfaces or target them for science activities. To maximize the diversity of analyzed targets, it is important for future UASs to possess the ability to point a landed science instrument and remotely target a feature of interest (e.g., via a robotic science arm; C. Rutter & M. Lach 2022) and have landing gear adaptable to rougher surfaces.
4. We developed a "reconnaissance-then-science" strategy using the oblique airborne images to scout a region of interest in advance of more intensive activity (i.e., surveying, landing, and landed science). The reconnaissance images helped improve flight safety, plan efficiency, and scientific return by identifying details not visible in the analog orbital data sets. This improved our ability to select ideal landing sites and targets for science activities. Advance scouting of landing sites from multiple perspectives was especially important.
5. Data collected by the UAS during its mission provided the key observations necessary to identify the spiny lava type of the younger lava flow field, fumaroles, and the flood deposit, as well as interpret their formation mechanisms. These detailed interpretations increased the scientific return of the UAS mission compared to what was possible with analog orbiter data alone.

Acknowledgments

We are grateful to the entire RAVEN Team for helping to develop and implement our analog science mission simulations. We acknowledge funding support from NASA PSTAR grant No. 80NSSC21K0011 and thank the Vatnajökull National Park Service (Vatnajökulsþjóðgarður) for providing permission to work in the Holuhraun region and the Icelandic Institute of Natural History (Náttúruminjasafn Íslands) for permission to export samples. This work was partially funded through a Canadian Space Agency FAST grant to C.N. (21FAUWOB01). This work was carried out in part at the Jet Propulsion Laboratory, California Institute of Technology, under a contract with the National Aeronautics and Space Administration.

Appendix
Raven UAS Mission LIBS Data

For each LIBS target identified by the UAS Science Operations Team, five scans were taken with the handheld LIBS instrument at the location by the UAS Field Implementation Team. The instrument reported scan results as elemental abundance in weight percent, which was then converted to oxide weight percent, shown in Table A1 as the normalized average for the five scans at each target.

Table A1
RAVEN UAS Mission LIBS Data

Code	Sol	Type	Al2O3 (%)	Al2O3 +/− (%)	CaO (%)	CaO +/− (%)	FeO (%)	FeO +/− (%)	K2O (%)	K2O +/− (%)	MgO (%)	MgO +/− (%)	MnO (%)	MnO +/− (%)	Na2O (%)	Na2O +/− (%)	SiO2 (%)	SiO2 +/− (%)	TiO2 (%)	TiO2 +/− (%)	Total Alkali (%)	Error	Total
SS_101	101	Landing Site	8.4574	0.0001	13.4456	0.0001	10.6464	0.0152	0.1343	0.0011	10.6351	0.0045	0.1808	0.0000	2.4735	0.0006	52.5258	0.0155	1.4529	0.0017	2.6078	0.0013	99.9517
SS_102	102	Sand Pre-Drill	8.5691	0.0254	13.4416	0.0002	12.1202	0.4055	0.1337	0.0018	10.7249	0.0076	0.1808	0.0000	2.4611	0.0025	52.4850	0.0125	1.4493	0.0015	2.5948	0.0031	101.5658
DS_103_a	103	Sand Claw	8.5203	0.0051	13.4410	0.0002	19.1960	0.6818	0.1648	0.0031	10.7790	0.0037	0.1808	0.0000	2.4335	0.0036	52.4843	0.0168	1.4688	0.0023	2.5982	0.0048	108.6684
DS_103_b	103	Sand Post-Drill	8.4574	0.0005	13.4445	0.0003	16.1247	0.4663	0.1203	0.0012	10.7147	0.0067	0.1808	0.0000	2.4879	0.0016	52.5963	0.0787	1.4650	0.0013	2.6081	0.0020	105.5915
SS_104	104	Sample Cache	8.4778	0.0093	13.4426	0.0002	14.1896	0.5621	0.1342	0.0019	10.7151	0.0059	0.1808	0.0000	2.4629	0.0031	52.4751	0.0076	1.4366	0.0012	2.5971	0.0036	103.5146
SL_105	105	Lava Pre-Drill	8.5311	0.0103	13.4438	0.0003	10.8775	0.1006	0.1990	0.0036	10.6250	0.0074	0.1808	0.0000	2.4583	0.0045	52.7411	0.0370	1.4395	0.0024	2.6574	0.0058	100.4962
DL_106	106	Lava Post-Drill	8.6987	0.0197	13.4448	0.0003	18.9259	0.5008	0.1556	0.0046	10.6908	0.0072	0.1808	0.0000	2.4203	0.0048	52.5807	0.0666	1.4549	0.0025	2.5759	0.0067	108.5524
AL_108	108	Deposit	8.7729	0.0210	13.4437	0.0003	22.2014	0.5465	0.1695	0.0031	10.6712	0.0101	0.1808	0.0000	2.4375	0.0030	52.5031	0.0145	1.4563	0.0021	2.6070	0.0044	111.8363
SL_110	110	Lava Pre-Drill	8.4875	0.0056	13.4438	0.0002	10.6907	0.0314	0.1582	0.0036	10.6234	0.0060	0.1808	0.0000	2.4391	0.0040	52.5596	0.0183	1.4343	0.0006	2.5973	0.0054	100.0173
DL_111	111	Lava Post-Drill	8.6513	0.0174	13.4469	0.0003	19.2337	0.5324	0.1213	0.0009	10.6648	0.0095	0.1808	0.0000	2.4524	0.0026	53.3070	0.1263	1.4630	0.0018	2.5737	0.0028	109.5213

ORCID iDs

Brett B. Carr https://orcid.org/0000-0002-1033-3082
Samantha Gwizd https://orcid.org/0000-0001-5818-9123
Catherine D. Neish https://orcid.org/0000-0003-3254-8348
Christopher W. Hamilton https://orcid.org/0000-0001-9731-517X

References

Adams, J. B., Pieters, C., & McCord, T. B. 1974, Orange Glass: Evidence for Regional Deposits of Pyroclastic Origin on the Moon, LPSC, 5, 171
Anderson, S. W., & Fink, J. H. 1992, Crease Structures: Indicators of Emplacement Rates and Ssurface Stress Regimes of Lava Flows, GSAB, 104, 615
Andresen, C. G., & Schultz-Fellenz, E. S. 2023, Change Detection Applications in the Earth Sciences Using UAS-Based Sensing: A Review and Future Opportunities, Drones, 7, 258
Balaram, J., Aung, M, & Golombek, M. P. 2021, The Ingenuity Helicopter on the Perseverance Rover, SSRv, 217, 56
Baniya, M. B., Asaeda, T., Shivaram, K. C., & Jayashanka, S. M. D. H. 2019, Hydraulic Parameters for Sediment Transport and Prediction of Suspended Sediment for Kali Gandaki River Basin, Himalaya, Nepal, Water, 11, 1229
Bapst, J., Parker, T. J., Balaram, J., et al. 2021, Mars Science Helicopter: Compelling Science Enabled by an Aerial Platform, BAAS, 53, 361
Barnes, Jason W., Turtle, Elizabeth P., Trainer, Melissa G., et al. 2021, Science Goals and Objectives for the Dragonfly Titan Rotorcraft Relocatable Lander, PSJ, 2, 130
Bonnefoy, L. E., Hamilton, C. W., Scheidt, S. P., et al. 2019, Landscape Evolution Associated with the 2014-2015 Holuhraun Eruption in Iceland, JVGR, 387, 106652
Bonny, E., Thordarson, T., Wright, R., Höskuldsson, A., & Jónsdóttir, I. 2018, The Volume of Lava Erupted During the 2014 to 2015 Eruption at Holuhraun, Iceland: A Comparison Between Satellite- and Ground-Based Measurements, JGRB, 123, 5412
Brady, A. L., Gibbons, E., Sehlke, A., et al. 2020, Microbial Community Distribution in Vvariously Altered Basalts: Insights into Astrobiology Sample Site Selection, P&SS, 194, 105107
Brockers, R., Delaune, J., Proenca, P., et al. 2021, Autonomous Safe Landing Site Detection for a Future Mars Science Helicopter, in 2021 IEEE Aerospace Conf. (Piscataway, NJ: IEEE), 50100
Broquet, A., & Andrews-Hanna, J. C. 2022, Geophysical Evidence for an Active Mantle Plume Underneath Elysium Planitia on Mars, NatAs, 7, 160
Burns, R. G. 1993, Mineralogical Applications of Crystal Field Theory (Cambridge: Cambridge Univ. Press)
Clarke, A. O. 1996, Estimating Probable Maximum Floods in the Upper Santa Ana Basin, Southern California, From Stream Boulder Size, EEGeo, II, 165
Cloutis, Edward A., & Gaffey, Michael J. 1991, Spectral-compositional Variations in the Constituent Minerals of Mafic and Ultramafic Assemblages and Remote Sensing Implications, EM&P, 53, 11
Costello, E. K., Halloy, S. R. P., Reed, S. C., Sowell, P., & Schmidt, S. K. 2009, Fumarole-Supported Islands of Biodiversity within a Hyperarid, High-Elevation Landscape on Socompa Volcano, Puna de Atacama, Andes, ApEnM, 75, 735
Farley, K. A., Williford, K. H., Stack, K. M., et al. 2020, Mars 2020 Mission Overview, SSRv, 216, 142
Francis, R., Estlin, T., Doran, G., et al. 2017, AEGIS Autonomous Targeting for ChemCam on Mars Science Laboratory: Deployment and Results of InitialSscience Team Use, Sci Robot., 2, eaan4582
Grotzinger, J. P., Crisp, J., Vasavada, A. R., et al. 2012, Mars Science Laboratory Mission and Science Investigation, SSRv, 170, 5
Gudmundsson, M. T., Jónsdóttir, K., Hooper, A., et al. 2016, Gradual Caldera Collapse at Bárdarbunga Volcano, Iceland, Regulated by Lateral Magma Outflow, Sci, 353, aaf8988
Gwizd, S., Stack, K. M., Francis, R., et al. 2024, Comparing Rover and Helicopter Planetary Mission Architectures in a Mars Analog Setting in Iceland, PSJ, 5, 172
Hadland, N., Hamilton, C. W., & Duhamel, S. 2024, Young Volcanic Terrains are Windows into Eearly Microbial Colonization, ComEE, 5, 114
Hartley, M. E., Thordarson, T., & de Joux, A. 2016, Postglacial Eruptive History of the Askja Region, North Iceland, BVol, 78, 28
Horn, B. K. P. 1981, Hill Shading and the Reflectance Map, IEEEP, 69, 14
James, Mike R., & Robson, Stuart 2014, Mitigating Systematic Error in Topographic Models Derived from UAV and Ground-based Image Networks, ESPL, 39, 1413
James, M. R., Carr, B., D'Arcy, F., et al. 2020, Volcanological Applications of Unoccupied Aircraft Systems (UAS): Developments, Strategies, and Future Challenges, Volca, 3, 67
Johnson, W., Withrow-Maser, S., Young, L., et al. 2020, Mars Science Helicopter Conceptual Design NASA/TM—2020–220485, NASA, https://ntrs.nasa.gov/citations/20200002139
Johnson, A. E., Cheng, Y., Trawny, N., et al. 2023, Implementation of a Map Relative Localization System for Planetary Landing, JGCD, 46, 618
Klima, R. L., Dyar, M. D., & Pieters, C. M. 2011, Near-infrared Spectra of Clinopyroxenes: Effects of Calcium Content and Crystal Structure, M&PS, 46, 379
Lancaster, N. 1994, Dune Morphology and Dynamics, Geomorphology of Desert Environments (Amsterdam: Springer), 474
Ljubicic, R., Strelnikova, D., Perks, M. T., et al. 2021, A Comparison of Tools and Techniques for Stabilising Unmanned Aerial System (UAS) Imagery for Surface Flow Observations, HESS, 25, 5105
Lorenz, R. D., Turtle, E. P., Barnes, J. W., et al. 2018, Dragonfly: a Rotorcraft Lander Concept for Scientific Exploration at Titan, John Hopkins APL Technical Digest, 34, 374, https://dragonfly.jhuapl.edu/News-and-Resources/docs/34_03-Lorenz.pdf
McEwen, A. S., Eliason, E. M., Bergstrom, J. W., et al. 2007, Mars Reconnaissance Orbiter's High Resolution Imaging Science Experiment (HiRISE), JGRE, 112, E05S02
MEPAG 2020, Mars Scientific Goals, Objectives, Investigations, and Priorities: 2020 Version White Paper, https://mepag.jpl.nasa.gov/reports/MEPAGGoals_2020_MainText_Final.pdf
Mier-Hicks, F., Grip, H. F., Kalantari, A., et al. 2023, Sample Recovery Helicopter, in 2023 IEEE Aerospace Conf. (Piscataway, NJ: IEEE), 1
Milkovich, S. M., Stack, K. M., Sun, V. Z., et al. 2022, Balancing Predictive and Reactive Science Planning for Mars 2020 Perseverance, in 2022 IEEE Aerospace Conf. (AERO) (Piscataway, NJ: IEEE), 1
Muirhead, B. K., Nicholas, A., & Umland, J. 2020, Mars Sample Return Mission Concept Status, in 2020 IEEE Aerospace Conf. (Piscataway, NJ: IEEE), 1
National Academies of Sciences, EngineeringMedicine 2023, Origins, Worlds, and Life: Planetary Science and Astrobiology in the Next Decade (Washington, DC: The National Academies Press),
Osinski, G. R., Battler, M., Caudill, C. M., et al. 2019, The CanMars Mars Sample Return analog mission, P&SS, 166, 110
Phillips, M., Tai Udovicic, C., Moersch, J., Basu, U., & Hamilton, C. 2024, HyPyRameter: A Python Toolbox to Calculate Spectral Parameters from Hyperspectral Reflectance Data
Pisanich, G., Plice, L., Ippolito, C., et al. 2004, Initial Efforts Toward Mission-representative Imaging Surveys from Aerial Explorers, Proc. SPIE, 5297, 106
Riley, S. J., DeGloria, S. D., & Elliot, R. 1999, A Terrain Ruggedness Index that Quantifies Topographic Heterogeneity, Int. J. Sci., 5, 23
Rowland, S. K., & Walker, G. P. L. 1987, Toothpaste Lava: Characteristics and Origin of a Lava Structural Type Transitional Between Pahoehoe and 'a'ā, BVol, 49, 631
Rutter, C., & Lach, M. 2022, Feasibility Study of a Robotic Science Arm on Future Martian Rotorcraft, in Presented at the VFS Aeromechanics for Advanced Vertical Flight Technical Meeting, Transformative Vertical Flight, San Jose, CA, Jan, 2022
Scheidt, S. P., & Hamilton, C. W. 2021, Unmanned Aerial System (UAS)-derived Orthoimage Mosaics and Digital Terrain Models of the Northeastern Portion of the 2014–2015 Holuhraun Lava Flow-field, Iceland: Data acquired from 2015 to 2018, v2, Univ.Arizona Research Data Repository. Collection, doi:10.25422/azu.data.c.5214641.v2
Schulze-Makuch, D., Wagner, D., Kounaves, S. P., et al. 2018, Transitory microbial habitat in the hyperarid Atacama Desert, PNAS, 115, 2670
Stahler, S. C., Mittelholz, A., Perrin, C., et al. 2022, Tectonics of Cerberus Fossae unveiled by marsquakes, NatAs, 6, 1376
Sutton, S. S., Chojnacki, M., McEwen, A. S., et al. 2022, Revealing Active Mars with HiRISE Digital Terrain Models, RemS, 14, 2403

Thordarson, T., & Larsen, G. 2007, Volcanism in Iceland in Historical Time: Volcano Types, Eruption Styles and Eruptive History, JGeo, 43, 118
Tmusic, G., Manfreda, S., Aasen, H., et al. 2020, Current Practices in UAS-based Environmental Monitoring, RemS, 12, 1001
Tolometti, G. D., Neish, C. D., Hamilton, C. W., et al. 2022, Differentiating Fissure-Fed Lava Flow Types and Facies Using RADAR and LiDAR: An Example From the 2014-2015 Holuhraun Lava Flow-Field, JGRB, 127
Vasavada, A. R. 2022, Mission Overview and Scientific Contributions from the Mars Science Laboratory Curiosity Rover After Eight Years of Surface Operations, SSRv, 218, 14
Velez-Nicolas, M., Garcia-Lopez, S., Barbero, L., Ruiz-Ortiz, V., & Sanchez-Bellon, Á. 2021, Applications of Unmanned Aerial Systems (UASs) in Hydrology: A Review, RemS, 13, 1359
Voigt, J. R. C., Hamilton, C. W., Keszthelyi, L. P., et al. 2024, PSJ, submitted
Voigt, J. R. C., Hamilton, C. W., Scheidt, S. P., et al. 2021a, Geomorphological Characterization of the 2014-2015 Holuhraun Lava Flow-field in Iceland, JVGR, 419, 107278
Voigt, J. R. C., Hamilton, C. W., Steinbrügge, G., & Scheidt, S. P. 2021b, Surface Roughness Characterization of the 2014-2015 Holuhraun Lava Flow-Field In Iceland: Implications for Facies Mapping and Remote Sensing, BVol, 83
Voigt, J. R. C., Hamilton, C. W., Steinbrugge, G., et al. 2022, Linking Lava Morphologies to Effusion Rates for the 2014-2015 Holuhraun Lava Flow Field, Iceland, Geo, 50, 71
Voigt, J. R. C., Hamilton, C. W., Steinbrügge, G., et al. 2023, Revealing Elysium Planitia's Young Geologic History: Constraints on Lava Emplacement, Areas, and Volumes, JGRE, 128, e2023JE007947
Wadge, G. 1981, The Variation of Magma Discharge during Basaltic Eruptions, JVGR, 11, 139
Wilson, M. F. J., O'Connell, B., Brown, C., Guinan, J. C., & Grehan, A. J. 2007, Multiscale Terrain Analysis of Multibeam Bathymetry Data for Habitat Mapping on the Continental Slope, MarGe, 30, 3
Yingst, R. A., Bartley, J. K., Chidsey, T. J., et al. 2020, Is a Linear or a Walkabout Protocol More Efficient When Using a Rover to Choose Biologically Relevant Samples in a Small Region of Interest?, AsBio, 20, 327
Young, L. A., Aiken, E. W., & Briggs, G. A. 2004, Smart Rotorcraft Field Assistants for Terrestrial and Planetary Science in 2004 IEEE Aerospace Conf. Proc. (IEEE Cat. No.04TH8720) (Piscataway, NJ: IEEE), 1
Young, L. A., Lee, P., Aiken, E., et al. 2021, The Future of Rotorcraft and Other Aerial Vehicles for Mars Exploration, in Vertical Flight Society's 77th Annual Forum & Technology Display, https://ntrs.nasa.gov/citations/20210014168